A low-cost and open-source olfactometer to precisely deliver single odours and odour mixtures

Connor Doyle[1], Jieni Wang[1,2], Elisa Galliano[1,*] Chloé Guillaume[1,*]

[1] Department of Physiology, Development and Neuroscience, University of Cambridge, United Kingdom [2] Department of Engineering, University of Cambridge, Cambridge, United Kingdom

* Correspondence to be addressed to Elisa Galliano (eg542@cam.ac.uk) or Chloé Guillaume (cg829@cam.ac.uk)

Abstract

Olfaction has historically been the neglected sense, despite its profound influence on human emotion and memory, and its critical importance for animal behaviours including foraging, mating, and parenting. Perhaps contributing to this neglect is the fact that olfactory research has been hindered by technical challenges inherent to odour delivery: unlike visual or auditory stimuli, odorants must be vaporized, transported, and actively cleared, requiring specialized equipment and creating temporal delays and contamination risks. While commercial olfactometers provide reliable solutions for odour delivery, they are expensive and, due to proprietary software, difficult to customize. Existing custom designs, though excellent, may also be costly and/or require access to engineering workshops. To widen access to controlled odour delivery and hopefully encourage more labs to undertake olfactory research, we developed a low-cost, fully open-source olfactometer system requiring no specialized workshops or extensive engineering expertise. Our design prioritizes affordability, accessibility, and versatility while maintaining temporal precision and stimulus control and supporting diverse applications from rodent behavioural studies to human psychophysical investigations. In this methods article, which includes design specifications and assembly instructions as well as validation data, we aim to lower barriers to olfactory research and enable more laboratories to explore this fundamental sensory modality.

Introduction

Olfaction has often been regarded as secondary to the other senses, in part due to the mistaken belief that the human sense of smell is weak compared to that of other animals (McGann, 2017). This false perception likely stemmed from the relatively small size of the human olfactory bulbs (Turner, 1890), which wrongly conflated anatomical size and functional impact. What remains is a true fundamental challenge in human olfactory research, namely the inherent difficulty of describing smells through language (Majid and Burenhult, 2014). However this linguistic gap does not imply a lack of functional importance: direct links from primary olfactory areas to brain regions such as the amygdala and prefrontal cortex (Shepherd, 2005) account for smell's profound influence on emotion and memory ("The memory of odors is very rich." East of Eden, John Steinbeck). And indeed attitudes have started to change on a larger scale following the COVID-19 pandemic, which caused a high incidence of comorbid anosmia and

heightened public awareness of how profoundly our quality of life depends on having a functional sense of smell (Xydakis et al., 2021), making human olfactory research both important and ripe for expansion. Conversely, rodents, one of the most widely used model organisms in neuroscience, have always been known to be deeply reliant on olfaction for a wide range of behaviours from foraging and predator avoidance (Nguyen et al., 2024) to mating (Ishii and Touhara, 2019) and parenting (Kohl et al., 2017). Given this ethological prominence in a such a widespread model organism, paired with unparalleled experimental accessibility of the rodent olfactory bulbs (large in size and dorsally located, making them prime real estate for physiological investigation at the neuronal level), it is striking that rodent olfaction remains understudied compared to sensory modalities such as vision.

Perhaps this relative lag in progress in olfactory research, both in humans and animal models, has been limited by a more practical issue: the difficulty of precisely controlling the delivery of olfactory stimuli. These technical challenges stem from the distinct physical and chemical properties of odorants. Unlike light or sound, which can be switched on and off almost instantaneously and delivered by screens and speakers bought in shopping malls, odour molecules must be vaporized, transported through the air, and then actively cleared, because they tend to linger after release. This creates delays between the onset or offset of a trial and the moment the odour reaches the test subject. Additional complications arise because of the need to generate pressure-controlled air flow to carry the odour, and in the limited ways that we have to detect and validate its delivery with pricey and generally user-unfriendly photoionization devices (PIDs). Moreover, many odorants adsorb to tubing, valves, or chamber walls, leading to contamination across trials and making reproducibility harder to guarantee.

Despite these difficulties, commercial and custom-made olfactometer designs that address many of these issues are available. Commercial olfactometers provide reliable, ready-to-use solutions, but they are often expensive (in the tens of thousands of dollars range) and may be difficult to adapt to specific experimental needs due to the closed nature of their software. The cost of these commercial systems becomes increasingly problematic if laboratories are interested in studying different aspects of olfaction, *e.g.* behavioural and neural level readouts on different setups, as they will therefore require multiple olfactometers. Many custom designs described in the literature are excellent, offering precise control, detailed construction guides, and thorough characterisation of their performance (Bodyak and Slotnick, 1999; Lorig et al., 1999; Johnson and Sobel, 2007; Lundström et al., 2010; Sezille et al., 2013; Burton et al., 2019; Reinert et al., 2019; Arevalo et al., 2025). However, none fully address all our key requirements: (1) affordable and scalable; (2) simple to assemble without specialised skills or access to mechanical/electronic workshops; (3) easily transportable across testing rooms or setups; (4) operated by fully open-source and customizable software; (5) suitable for a variety of experimental configurations, ranging from human imaging experiments in a scanner, to rodent freely moving and head-fixed behavioural experiments; (6) suitable for multi-subject setups for simultaneous testing; (7) capable of delivering both single odours and mixtures while maintaining constant air pressure.

To address this and democratize access to controlled odour delivery, and thus hopefully help increase the footprint of olfactory research, we have developed a low-cost, fully open-source olfactometer system that can be assembled and operated without specialized workshops or extensive engineering expertise. Our design prioritizes affordability, accessibility, and versatility while maintaining the temporal precision and stimulus control required for rigorous research. The system is suitable for a wide range of experimental applications, from basic rodent behavioural studies to human psychophysical investigations, and can be adapted to diverse experimental needs. In this article, we provide complete design specifications, assembly instructions, validation data (both olfactometric

and behavioural), and operational protocols for the olfactometer and associated rodent behavioural chambers. By making these resources freely available, we aim to lower the barriers to conducting olfactory research and enable more laboratories to explore the rich scientific questions that can be addressed in different models. Additionally, we hope that others can take our design as inspiration and adapt and extend it, and share their improvements in keeping with the open-science ethos of this work.

Results

Design

Our olfactometer consists of three core components: (1) a continuous air supply that maintains the desired flow rate, (2) a set of four modules, each containing one solvent bottle and one odour bottle where liquid odorants at the desired dilution are vaporised, with the option for further expansion, (3) a digital control system that regulates both which odours are delivered and the timing of their delivery via solenoid valves installed on each bottle, all operated through open-source software running on a standard computer. The design ensures that a clean carrier stream is always present at the output. Meanwhile, air flowing into sealed solvent or odour bottles becomes saturated with vapour but remains contained until the software triggers the opening of its corresponding solenoid valve. When the valve opens, the odourised air merges with the carrier flow and is delivered to the output. In this way, the four-module olfactometer can present clean air, single odours, or controlled mixtures (up to four simultaneously) at defined concentrations and durations (Figure 1B).

Air supply system

Controlled odour delivery requires first injecting air to vaporise the odorants, then transporting them via a stable air stream. The air source may be either a medical compressor, or an oxygen/medical air cylinder, or, if suitably clean and available, pressurized air from wall taps, such as those used to inflate optical tables. From the source, the air is divided into two streams, a carrier path and an odour path, with independent pressure regulators (0.2 MPa each). From the pressure regulator, the carrier stream passes through a dedicated flowmeter (1 L/min) and bypasses all odour modules, flowing continuously to the output (Figure 1B). This maintains a stable baseline and flushes residual vapours between trials. From the odour path regulator, the odour stream splits and passes through four flowmeters (0.3 L/min each), feeding four independent odour modules. Within each module, air is directed through solvent and odour bottles, the inner air becoming saturated but remaining sealed until its solenoid valve is triggered via the desktop PC.

Odours tend to linger after release, creating a risk of cross-contamination between trials. In our design this contamination is minimized by the continuous carrier air stream which helps to clear odorants from the olfactometer itself. However, if the output area in the testing apparatus is small and/or enclosed (behaviour chambers, masks, etc.) it is recommended to include a vacuum extraction system to quickly remove residual odours from these contaminated areas after each trial.

Odour modules

Our odour module design is adapted from Rokni et al., (2014). Each module comprises two sealed bottles: one containing solvent and one containing odorant. With four modules total, the system holds eight bottles (four solvent, four odour), with the modules colour-coded Red, Blue, Green, and White for reference (Figure 1B). Each bottle is fitted with

two needles: an inlet connected to the air supply and an outlet linked to a solenoid valve and air output (Figure 1A). When the valve is closed, saturated air accumulates at low pressure within the bottle; when opened, the odourised air is released and merges with the carrier flow. A key feature of this paired design is that it maintains constant air pressure at the output when odours are released. When only one odour is presented (*e.g.*, Red module), the solenoid valves of the other modules open their solvent bottles. This ensures that the total number of open bottles is constant across trials, preventing differences in airflow pressure between single-odour and odour mixture conditions.

Electronic control of olfactometer

Odour delivery is controlled using an Arduino-compatible microcontroller programmed via the Arduino integrated development environment (IDE, version 2.3.5) on a desktop PC (Figure 1A). The Arduino provides 5V digital timing signals to valve driver boards, which then supply the necessary power to open or close the solenoid valves in each module. Each valve driver board has two identical valve control circuits, thus can operate one complete module (*i.e.*, one odour and one solvent bottle). Thus for our four-module (Red, Blue, Green, White) design, four valve driver boards are required. Because the Arduino-compatible microcontroller only provides the control signal, a power converter board is required to supply the voltages necessary for valve actuation. Each power converter board steps down a 12 V supply into two 2.8 V and two 7 V lines, providing the power needed to open and hold the solenoid valves. Two power converter boards are sufficient for the standard four-module setup, though the system can be scaled to additional modules if required.

Below we detail the necessary steps to construct this complete system, including how to build the electronic boards (valve driver boards and power converter boards), and the air flow control which is then attached to the odour bottles. All parts are commercially available, their references are listed in Table 1.

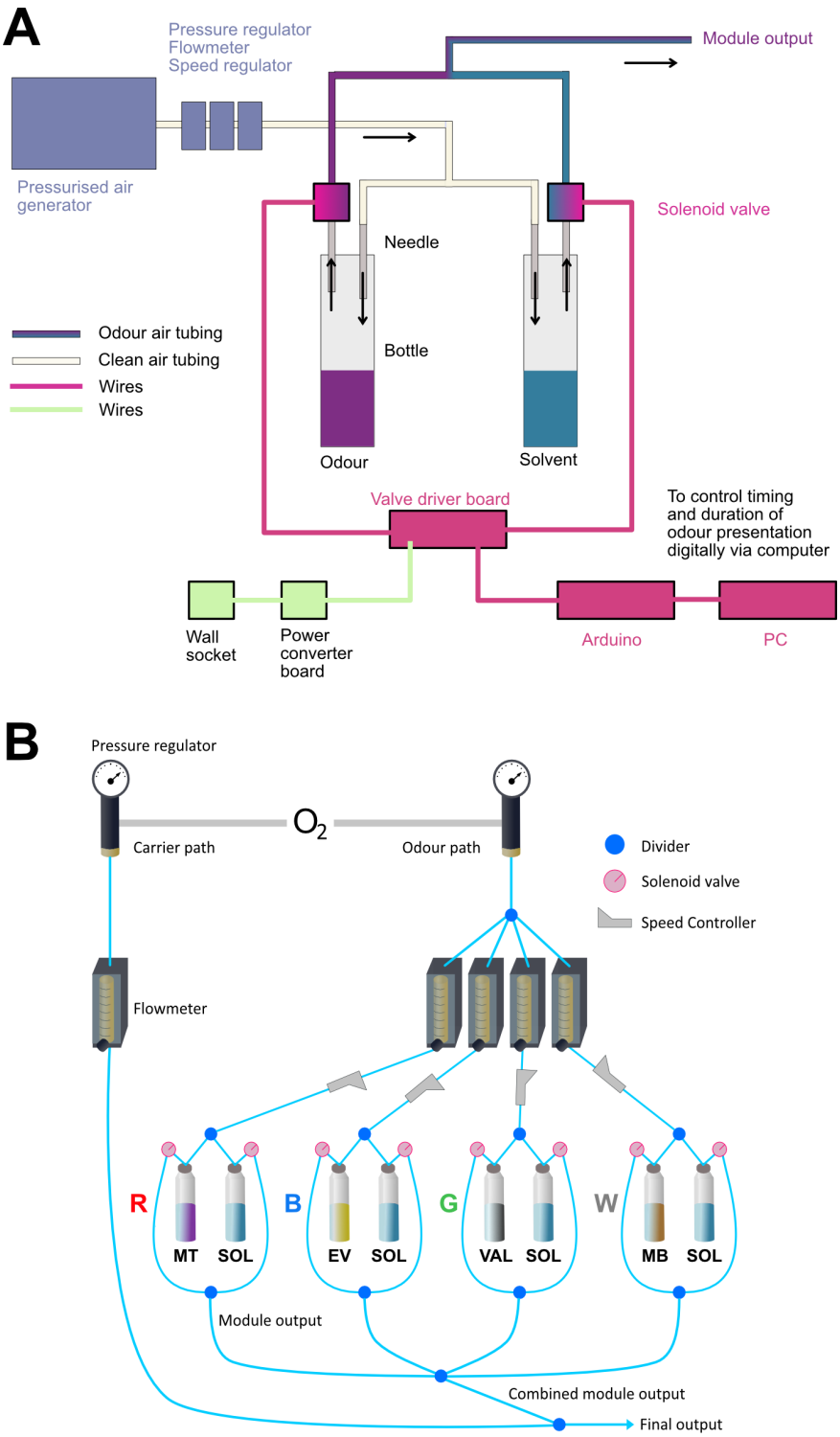

Figure 1. Olfactometer design and operation. (A) System overview showing the three main components: air supply system (blue), detailed view of a single odour module showing the paired bottle design with air flow control systems, inlet/outlet needles, solenoid valve control, and integration with the Arduino-based control system via valve driver boards and power converter boards (magenta and green). (B) Schematic representation of the air flow system across the four colour-coded odour modules (Red, Blue, Green, White) each containing paired solvent (SOL) and odorant bottles, and electronic control via solenoid valves. The carrier stream (1 L/min) flows continuously to maintain stable baseline conditions, while odour streams (0.3 L/min each) pass through individual modules before merging at the output. Abbreviations: MT, methyl tiglate; EV, ethyl valerate; VAL, valeraldehyde; MB, methyl butyrate.

Construction

Air supply system

Before starting, please note that the tubing lengths are only provided as a guide and should be adapted to best fit your setup. If tubing lengths are adapted it is key to try and make the total tubing length as short as possible and to ensure the tubing length is consistent across modules to avoid low output or differences in airflow. Additionally, the size of the input air flow tubing and adaptors may need to be adapted to match the output of your air supply system (*e.g.*, our medical air compressor utilises a 6mm output). See component list in Table 1 and schematic in Figure 2 for further guidance. Please note that no glue is needed, you just need to tightly force the connectors into the tubing.

1. Take two pneumatic pressure regulators (SNC, AR20-F01BG-B). For the odour path regulator, attach G1/8-to-6mm adaptors (RS Components, 299-3819) to both the input and output ports. For the carrier path pressure regulator, attach a G1/8-to-6mm adaptor (RS Components, 299-3819) to the input port and a G1/8-to-4mm adaptor (RS Components, 3796) to the output port (Figure 2A, left).

2. Take a 6mm Y connector (RS Components, 916-0918) and attach two ∼25cm pieces of 6mm polyether tubing to its two-pronged end. Connect the other end of the polyether tubings to the input connectors of both pressure regulators (Figure 2A, right). Using 6mm tubing, connect the air compressor (MGF compressors, S-OF100-003-MS2) to the Y connector.

3. Take five flowmeters (Key Instruments, 25102A13BVBN) and to each securely attach two elbow adaptors (SMC, KQ2L03-34AS; Figure 2Bi). One flowmeter is for the carrier path, the other four are for each odour module. It may be useful to colour coordinate the flowmeters (see Figure 2C).

4. Securely fix the five flowmeters, to the shelf of a trolley, or your desired structure (Figure 2Bii). Connect a piece of 4mm tubing (∼30cm length) from the output port of the carrier path pressure regulator to the bottom (input) elbow adapter of the carrier path flowmeter (Figure 2C).

5. Take a double Y connector (6mm to 4mm, Festo, QSQ-6-4) and connect it to the output port of the odour path pressure regulator using a ∼10cm piece of 6mm tubing.

6. Use ∼30cm of 4mm tubing to connect each of the four odour module flowmeters (via the bottom elbow adaptor) to the double Y connector (Figure 2C).

7. Attach ∼30cm 4mm tubing to the top (output) elbow adaptor of each of the four odour flowmeters. Connect each flowmeter to a separate speed controller (SMC, AS1211F-M5-04).

8. To each speed controller, attach an M5 to 4mm adaptor (RS components, 176-1293). Use a small piece of 4mm (∼2cm) tubing to connect each speed regulator to a 4mm Y connector (RS Components, 916-0915; Figure 2Biii).

9. Attach ∼20cm 4mm tubing to the two-pronged end of the 4mm Y connector. These tubings will deliver air to the odour bottles (Figure 2Biii).

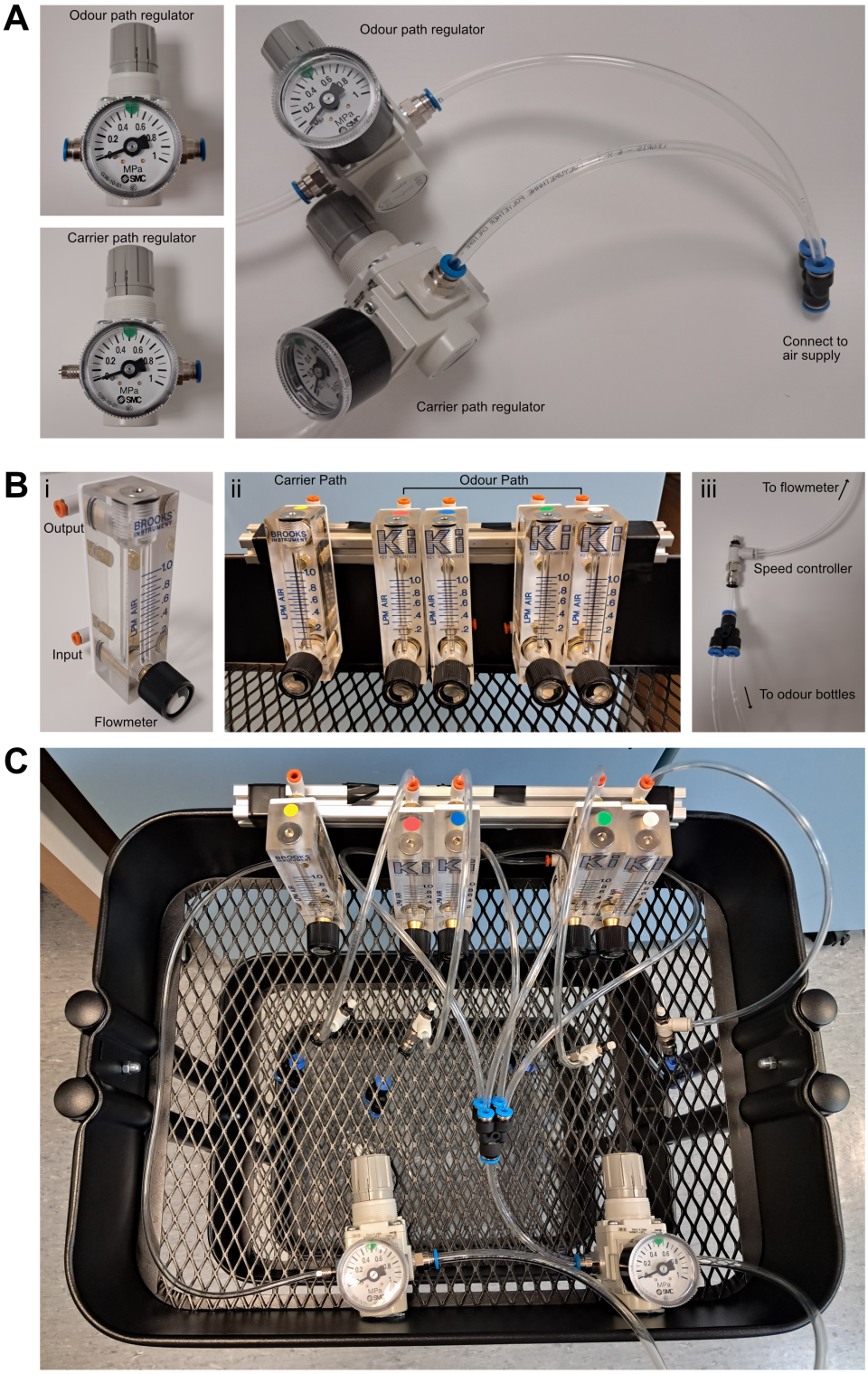

Figure 2. Air supply and regulation for the olfactometer. (A) Left: Pressure regulators for the carrier and odour paths, with Right: tubing connecting the regulators to the air supply (*e.g.*, air compressor). (B) i) Flowmeter with input and output connections highlighted. ii) All five flowmeters attached to the olfactometer trolley. iii) Speed controller connecting the flowmeter to the odour bottles. (D) Complete air supply system.

Odour modules

See component list in Table 1 and schematic in Figure 3 for more information. We selected these bottles, caps, and needles after testing multiple alternatives. Screw-on caps were essential as snap-on versions failed under operating pressure. The silicone-sealed caps maintain integrity when pierced while minimising leakage. The 40ml brown glass bottles provide optimal volume as larger bottles require excessive odorant for adequate vapor concentration, while smaller ones cannot withstand operating pressures without valve failure nor enable the use of solid material (*e.g.*, coffee beans). Brown glass protects light-sensitive odorants. While our testing was thorough, other suitable combinations may exist.

1. Attach screw top lids (Fisher Scientific Ltd, 10729454) to 8 odour bottles (Fisher Scientific Ltd, 11530585).
2. Carefully insert two 19g syringe needles (Appleton Woods Ltd, GS357) through the lid of each bottle (Figure 3, top left). Unscrew the lid (with needle attached) and clear any rubber from the needle by blowing out with a 15ml syringe.
3. Attach a barbed 3/32"to-male Luer adaptor (Fisher Scientific Ltd, 16894673) to the inlet of each needle (Figure 3, top left).
4. Connect a small (∼2cm) piece of 4mm tubing to one of the needles on each bottle. This is the bottle output. To the other needle, attach the tubing from Air flow control, step 9. This is the bottle input (Figure 3, middle).
5. Attach the top connector of a solenoid valve (Lee Company, LHDB1262245D; Figure 3, bottom left) to the bottle output tubing. Connect the solenoid valves to the valve driver board built earlier with a jumper wire at the position indicated in Figure 4B.
6. Attach a ∼15cm long 4mm tubing to the bottom connector of the solenoid valve. This is the valve output tubing (Figure 3, right).
7. Use a 4mm Y connector (RS Components, 916-0915) to combine the valve output tubing from one solvent and one odour bottle, forming a module (Figure 3, right).
8. Repeat this process for the remaining three modules.
9. Use a Double-Y Tube-to-Tube adaptor (push in 4mm-to-push in 4mm) to combine the four output tubings from the four modules into a single odour line.
10. Use a 4mm Y connector to connect the combined odour line with the top elbow adaptor from the carrier path flowmeter.
11. Attach the final output tubing (4mm) to the single-end of the 4mm Y connector. This delivers the final odour mixture to the arena.
12. Before starting the experiment, add pure solvent to solvent bottles, and odour diluted as required in solvent to odour bottles. We use 1ml per bottle, but this can be altered as long as the liquid level remains below the needle tips. Alternatively, solid odour sources such as coffee beans could be used instead.

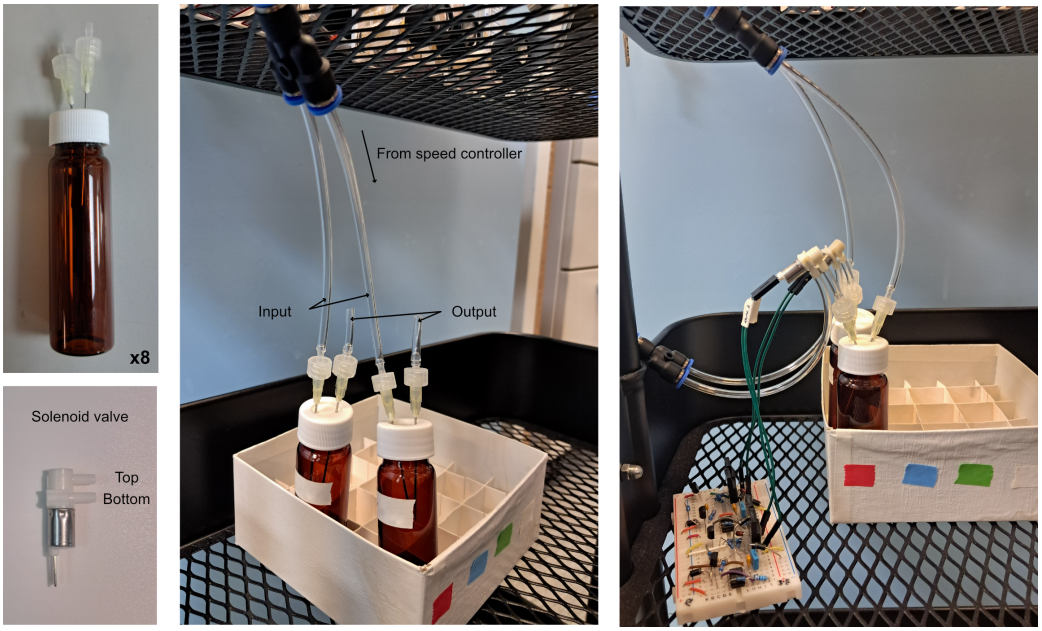

Figure 3. Odour and solvent bottle assembly. Top left: capped odour bottle with attached needles. Bottom left: Valve with connections labelled. Middle: odour and solvent bottles for the Red module, with tubing from Fig 2Biii connected to the bottle inputs. Right: connection between bottles and solenoid valves mounted on the valve driver board.

Electronic boards

1. Build power converter boards using the component list in Table 1 and schematic in Figure 4A. The standard setup requires two converter boards (each powers two valve driver boards). No soldering needed, simply insert the pins into the correct holes.

2. Build valve driver boards using the component list in Table 1 and schematic in Figure 4B. The standard setup requires four valve driver boards (1 per module). No soldering needed, simply insert the pins into the correct holes.

3. Connect power convertor and valve driver boards (see Figure 4A and 4B for further guidance)

   (a) Connect 7V output (converter) to 7V rail (valve driver)

   (b) Connect 2.8V output (converter) to 2.8V rail (valve driver)

   (c) Connect ground (GND) rail (converter) to GND rail (valve driver)

   (d) Connect 12V rail (converter) to 12V rail (valve driver)

Power supply system

1. Cut two ∼6cm strands of hookup wire (Farnell, Alpha Wire 2290891). Use wire strippers to reveal a couple millimetres of wire at each end.

2. Solder jumper wires (Farnell, Bud Industries 2762508) to one end of each hookup wire (we use a green jumper wire for ground, and a red jumper wire for 12V).

3. Use heat shrink tubing to protect the soldering join by cutting a piece of appropriate length, placing it over the join, and using heat from a lighter or similar to make it shrink and adhere.

4. Screw the opposite ends of the hookup wires to the power socket-to-screw terminal adaptor (CPC, Clever Little Box CLB-JL-53) - green jumper wire to negative terminal, red jumper wire to the positive terminal.

5. Connect 12V power supply (CPC, Ideal Power PW04341) to the screw terminal adapter (Figure 4E).

6. Connect red jumper (12V) to positive rail of converter board.

7. Connect green jumper (GND) to negative rail of converter board.

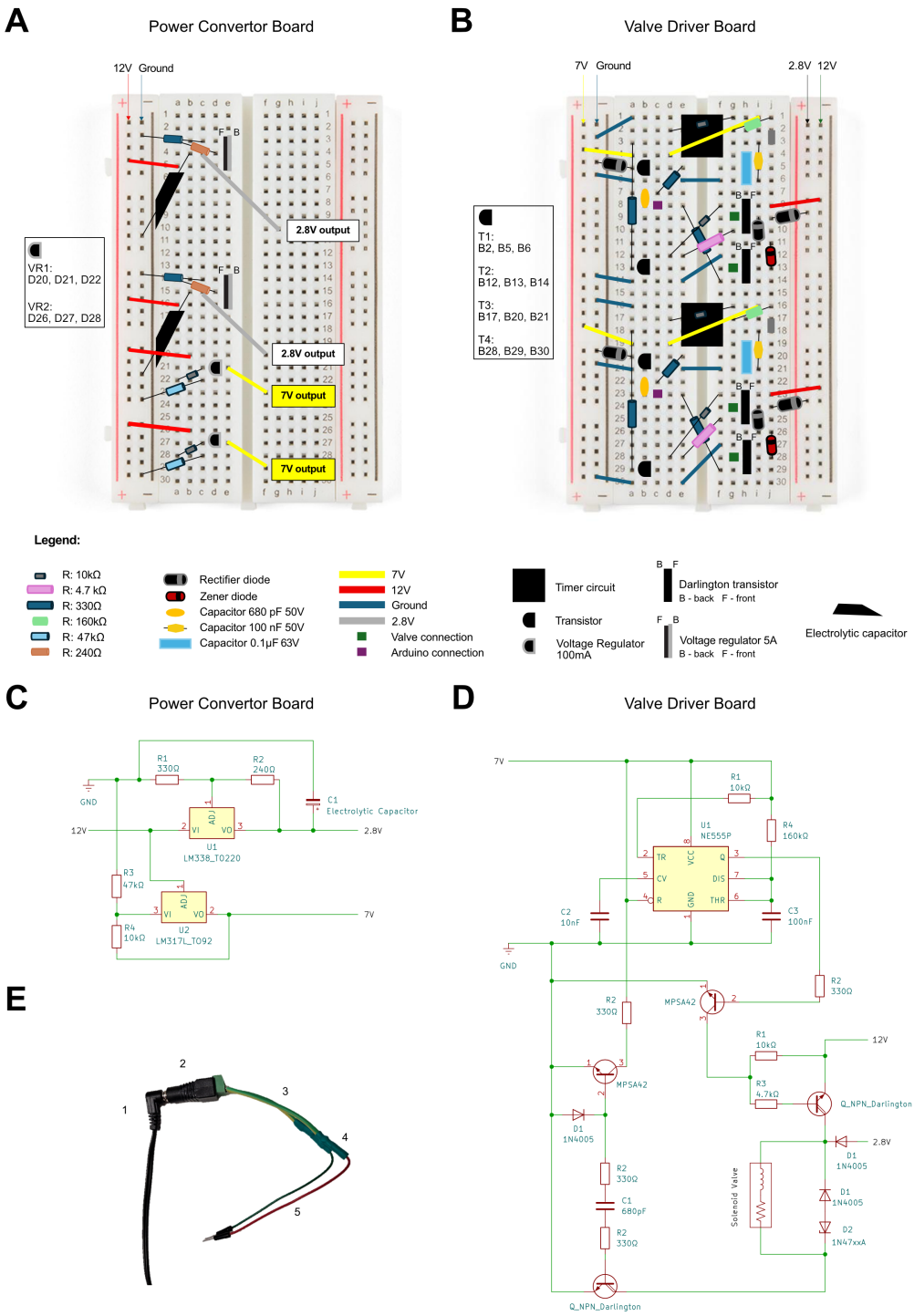

Figure 4. Electronic components required for running the olfactometer. (A) Diagram of the power converter board, which converts a 12 V power supply into two 2.8 V and two 7 V lines to power the valve driver boards. Box indicates the placement of the three legs of voltage regulators, VR1 and VR2. Each converter board powers two valve driver boards. (B) Diagram of the valve driver board, which controls solenoid valve opening and thus odour delivery. Each valve driver board consists of two circuits: rows 1–14 control one valve, and rows 16–30 control a second valve. Box indicates the placement of the three legs of transistors T1–T4. A legend of all components used in panels A and B is shown below. (C) Electronic schematic of the power converter board showing one 2.8V circuit (*e.g.*, lines 2-11 of panel A) and one 7V circuit (*e.g.*, lines 20-24 of panel A). (D) Electronic schematic of one circuit (*e.g.*, rows 1-14) of valve driver board. (E) Image of the power supply setup for the converter boards, showing: (1) 12 V power supply, (2) power socket-to-screw adaptor, (3) hookup wires, (4) soldering joint with heat-shrink tubing, and (5) male-to-male jumper wires.

Optional step: Construct behavioural arenas for rodent experiments

Upon completing the steps above, you will have a functional olfactometer capable of delivering odours. However, these odours require a delivery destination. The olfactometer's final output uses standard 4mm polyurethane tubing, which can be connected to various delivery systems. Below, we describe the construction steps for the behavioural arenas we developed and validated. It is important to note that replicating this specific system is not required to utilise the olfactometer effectively, we provide these details merely as a reference for interested researchers and highlight that the dimensions can be easily altered to fit animal models bigger than mice. Alternative delivery methods may include connections to masks (Johnson and Sobel, 2007) or nosepieces for human subjects (Lundström et al., 2010). The protocol below describes the construction of a single behavioural arena. This design can be scaled as required, we have successfully constructed and validated four arenas operating simultaneously from one olfactometer. If relevant for your experiment, please see Table 2 and Figure 5 for more details.

1. To form a hole for an odour port, drill a 5cm hole approximately 5cm from the bottom of a Black Cast Perspex Acrylic Sheet (300mm × 200mm × 3mm; Figure 5A).

2. To form a hole for the vacuum exhaust, drill a 0.5cm hole approximately 5cm from the top of a second Black Cast Perspex Acrylic Sheet (300mm × 200mm; Figure 5B).

3. Half-way up one Black Cast Perspex Acrylic Sheet (300mm × 300mm), attach a 10cm length of aluminium angle (RS, 681-716) using superglue. Allow to dry.

4. Glue the Black Cast Perspex Acrylic Sheet (300mm × 200mm) with the odour port hole (from step 1) to the other side of the aluminium angle.

5. Repeat this process with a second Black Cast Perspex Acrylic Sheet (300mm × 300mm) to form a three-walled structure, with the odour port hole located on the short wall (Figure 5A).

6. Glue two approximately 10cm lengths of aluminium angle along the lower edges of the walls, leaving ∼4 cm clearance from the base to allow the floor to slide under.

7. Insert a small funnel (Fogcays, 3xgf) into the odour port; secure with tape, glue to form the odour port.

8. Wrap a Clear Cast Perspex Acrylic Sheet (300mm × 195mm) in Polythene backed absorbent protector sheet (Benchkote, 2300-916) and slide into the chamber. The absorbent sheet helps track mouse scent-marking and aids with cleaning, and may be skipped.

9. Insert the Black Cast Perspex Acrylic Sheet (300mm × 200mm) with the exhaust hole (from step 2) as the fourth wall and secure it with tape or Blu-Tack.

10. Cut the aluminium profile strut (RS, 8508476) into two 5cm lengths. Attach these securely near the roof of the box adjacent to the wall containing the exhaust hole. This will hold the wall in place.

11. Connect the olfactometer output tubing directly to the neck of the odour port using a small piece of 4mm ID polyurethane tubing (RS Components, 366-459; see Figure 5D).

12. Attach two barbed connectors (Harvard Apparatus, 72-1500) to the input and output ports of the LD10 Linear Diaphragm Pump (Charles Austen Pumps Ltd, X12-810). Connect a ∼3 cm length of 4 mm tubing (RS Components, 917-2407) to the output connector. For the input connector, attach a longer piece of 4 mm tubing that extends to the behavioural arena, with one end inserted into the exhaust hole and the other secured to the pump's input connector (Figure 5C).

13. Insert a straight reducer (Cole-Parmer, 5010881) into the end of the tubing inside the box to secure it and prevent the tubing from slipping out during experiments.

14. Place a Black Cast Perspex Acrylic Sheet (300mm x 205mm) on top of the arena to form an enclosed, dark space during experiments.

For multi-arena setups, use Y-adaptors to divide the olfactometer output across multiple arenas. Provide exhaust ventilation for each arena using multiple LD10 Linear Diaphragm Pumps with the appropriate splitting adaptors. In our setup, a single pump is used to ventilate two arenas.

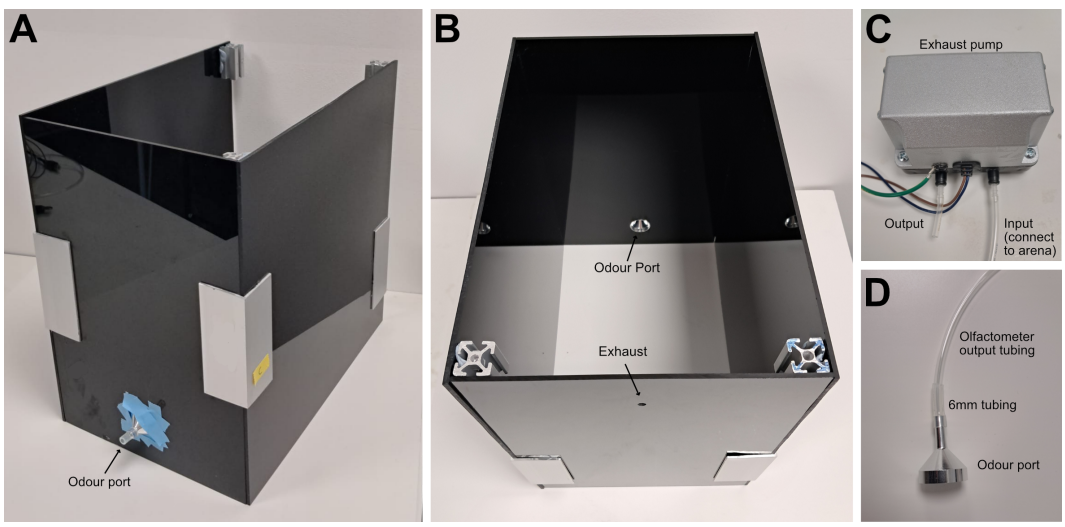

Figure 5. Behavioural arena construction and odour delivery system. (A) Three-walled behavioural arena with attached odour port. (B) Alternative view showing the exhaust hole for residual odour removal. (C) Linear diaphragm pump for arena ventilation, with input and output connections labelled. (D) Close-up view of the odour port connection to olfactometer output tubing.

Optional step: Camera setup

In the following section, we describe the setup of cameras used to monitor behaviour in our arenas. It is important to note that cameras are not required to operate the olfactometer, and we provide these details as a guide for those who may find them useful. This protocol outlines the camera setup for a single behavioural arena, using one overhead and one side-view camera. For multiple arenas, we recommend a separate side-view camera for each, and testing whether a single overhead camera can capture all arenas within frame. If not, an additional overhead camera may be required. Cameras may also be of interest for psychophysical experiments to track human facial features indicative of alertness such as pupil size (Park and Whang, 2018).

1. Place the pre-built behavioural arena onto a table. Tighten the tabletop camera mount stand (NEEWER, TL253A+CR221A) to the table.

2. Screw the topview camera (Svpro, SVB-USBFHD05MT-KL36IR) to the tabletop mount stand. Plug camera USB cable into a desktop PC.

3. Assemble the helping hands (JZK, M461328U) and attach the non-slip base to the table. Using the provided clips, hold the sideview camera (Arducam, B0205) in place. Plug camera USB cable into a desktop PC.

4. Both topview and sideview cameras have built in IR lights, depending on your setup it may be necessary to cover these to prevent glare.

Software for performing experiments

Controlling odour delivery

1. Connect the Arduino-compatible microcontroller to a desktop PC or laptop.

2. Using jumper wires, link the Arduino digital output pins to the appropriate rows on the valve driver board (*e.g.,* connect digital pin 2 to row 23 of the red module valve driver board for the odour valve, and digital pin 3 to row 8 for the solvent valve; Figure 4B). Connect the Arduino GND to the GND line of the power converter board.

3. Download and install the Arduino IDE (arduino.cc/en/software). Open the IDE and select the correct board model under *Tools* > *Board*.

4. Write a custom script to define the desired odour delivery sequence, verifying that the pin numbers specified in the code match the physical wiring.

5. Switch on the 12 V power supply at the socket. Start the olfactometer by uploading the script (*Upload* in the Arduino IDE).

6. (Optional) For experiments involving behavioural video recording, an LED can be added within the camera's field of view and controlled by the Arduino to illuminate whenever an odour valve is opened. This provides a clear temporal marker to verify which odour bottle was active during analysis.

For more information on Arduino programming, visit here (`https://docs.arduino.cc/software/ide/`). As an example, the following demonstrates how to control a solenoid valve connected to Arduino digital pin 2.

```
int odourPin = 2; // Defines digital pin 2 as the pin used to control the solenoid valve

void setup() {
pinMode(odourPin, OUTPUT); // Declares pin 2 an output, allowing it to send voltage to the valve.
digitalWrite(odourPin, LOW); // Sets pin 2 to low voltage state, so valve is initially closed.
}

void loop(){
digitalWrite(odourPin, HIGH); // Sets pin 2 to a high voltage state (5V), opening the valve.
delay(1000); // Holds valve open for 1000ms (1 second)
digitalWrite(odourPin, LOW); // Returns pin 2 to a low voltage state, closing the valve.
delay(10000); // Pauses execution for 10 seconds, keeping valve closed until the loop restarts
}
```

Recording and synchronising videos

This section outlines how to record and synchronise video from one or more cameras during experiments using a single behavioural arena in Bonsai-rx (Lopes et al., 2015). The protocol is provided as a guide and is entirely optional. The workflow can be adapted for multiple arenas, allowing simultaneous capture from overhead and side-view cameras or other camera arrangements.

1. Download (`https://bonsai-rx.org/docs/articles/installation.html`) and launch Bonsai-rx on a laptop or desktop PC.

2. Create a new project and add two `VideoCaptureDevice` nodes. Assign each node to each camera in the setup (one for overhead, one for sideview) and configure frame size and framerate.

3. Connect both `VideoCaptureDevice` nodes to a `WithLatestFrom` node. Connect this node to a `Concat` node and then to a `VideoWriter` node (see Lopes and Monteiro, 2021 for more help).

4. Disable the `VideoWriter` nodes (Ctrl+D) and press `Start` to preview the camera feeds. Adjust camera position/setting as required. Re-enable `VideoWriter` nodes (Ctrl+Shift+D).

5. When ready to begin the experiment, press `Start` to begin video acquisition.

Validation of basic function

We first validated whether our olfactometer could deliver reliable odour signals that were both stable across repeated presentations and tightly coupled to valve actuation. Using a miniPID (Aurora Scientific, 200B), we recorded responses to ten consecutive 10s presentations of 1ml 5% methyl tiglate (MT) in diethyl phthalate (DP) solvent. The traces exhibited a stereotyped waveform characterised by a rapid peak following valve opening, a stable plateau during odour delivery, and a sharp return to baseline upon valve closure (Figure 6Ai). Quantification (Figure 6Aii-iv) confirmed consistent peak amplitude (mean ± SD, 83.86 ± 1.25mV), plateau amplitude (mean ± SD, 25.48 ± 0.30mV) and response latency (mean ± SD, 65.72 ± 1.81ms) across 10 trials.

Having access to a commercially available computer-controlled olfactometer (CyNexo srl, Sniff-0), we next compared the performance of our custom olfactometer to the Sniff-0 device. With the commercially available olfactometer, 2s presentations of 1ml 5% valeraldehyde (VAL) produced square, step-like miniPID responses with large amplitude signals (Figure 6Bi-ii; mean ± SD, 457.05 ± 67.82mV). In contrast, our olfactometer produced consistent peak-plateau responses, similar to those recorded with 5% MT, during 5s presentations of 1ml 5% VAL, with lower yet comparable peak amplitudes (Figure 6Bi-ii; mean ± SD, 352.88 ± 2.37mV).

Having confirmed that our olfactometer can be used to reliably deliver odorants, we next investigated whether the concentrations delivered by our olfactometer are relevant behaviourally. To evaluate this, we utilised a habituation-dishabituation task, a standard task used to assess the ability of a mouse to discriminate between two odours (Zou et al., 2015; Conway et al., 2024). Mice were placed in the custom-built behavioural arena (Figure 6Ci), with odours delivered through an odour port connected to the olfactometer. IR cameras were used to record their behaviour. Once in the chamber, mice were exposed to five 60s presentations of solvent, with 30s intertrial intervals (Figure 6Cii), before being exposed to three 60s presentations of 5% MT. After habituating to solvent, we observed a significant increase in investigation during the first presentation of MT (Figure 6Ciii; 5th solvent, mean ± SEM = 2.19 ± 0.67s; 1st MT = 6.60 ± 1.64s; paired t-test, $t(5) = -3.19$, $p = 0.024$), indicating the mice were able to detect and discriminate the odour delivered from the olfactometer compared to the solvent.

In summary, while our olfactometer yields different waveforms and lower peak amplitudes compared to a commercial olfactometer, it reliably produces detectable odour signals with short latencies following valve actuation and excellent trial-to-trial stability. Additionally, the behavioural experiment provides biological validation of the appropriateness of our olfactometer.

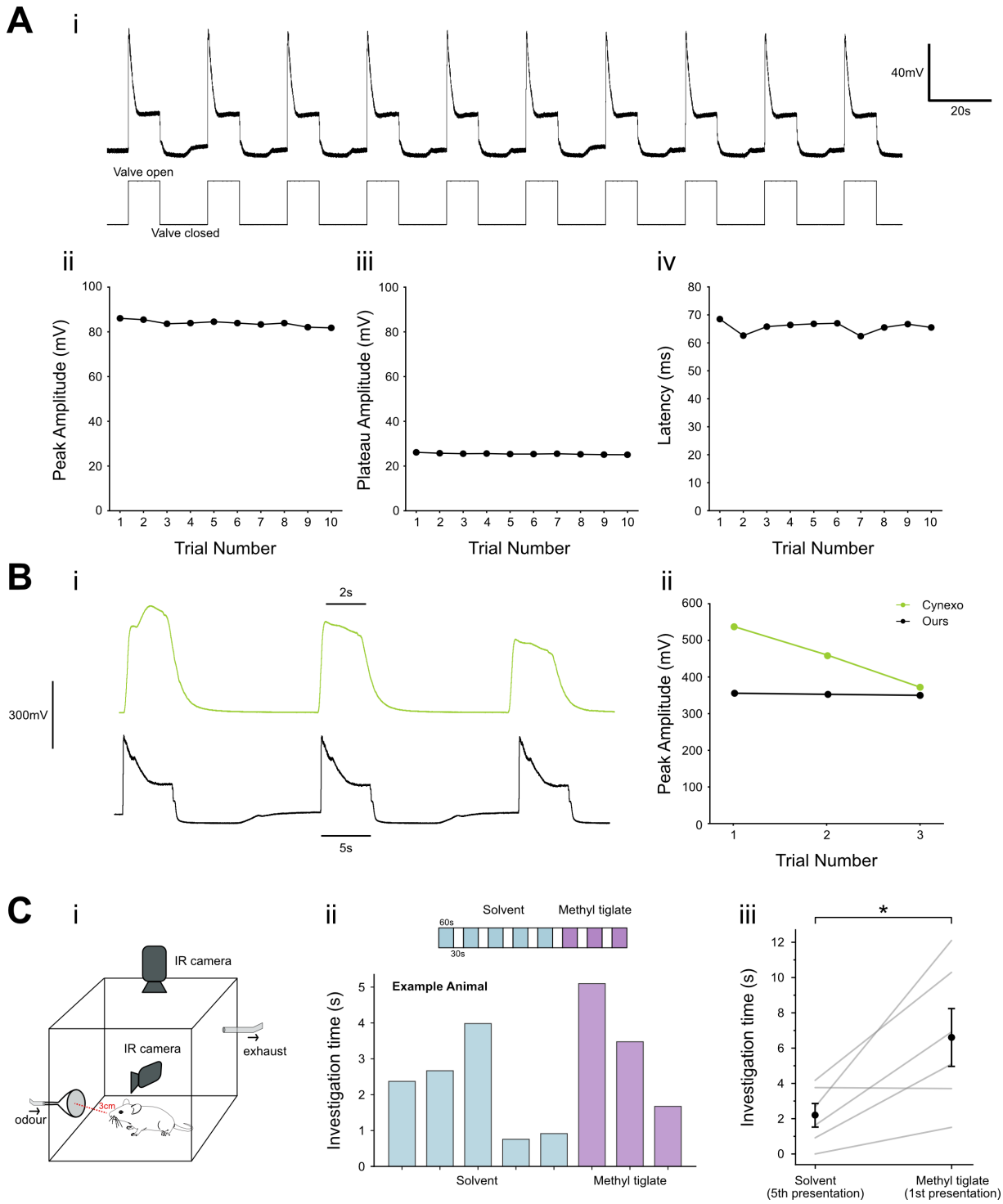

Figure 6. Odour delivery controlled by the olfactometer. (Ai) Complete recording trace of 5% methyl tiglate (MT) from a single module across ten 10s presentations. Top: miniPID signal; bottom: digital output voltage trace from Arduino indicating the timing of valve opening. (Aii–iv) Quantified features include (i) peak amplitude, (ii) plateau amplitude, and (iii) latency from valve actuation to peak amplitude. (Bi) Representative PID traces of 5% valeraldehyde (VAL) from CyNexo srl and our olfactometer. (Bii) Quantification of peak amplitude. (Ci) Experimental paradigm; mice were placed in a behavioural arena with an odour delivery port and an exhaust fan to remove odours. IR cameras were used to record behaviour and track investigations (mouse nose within 3cm of odour port). (Cii) Above: Experiment protocol; the coloured blocks represent 60s of solvent or MT delivery, with 30s intertrial interval. Below: Bar plots of odour port investigation duration of one example animal across the whole experiment. (Ciii) Odour investigation times during fifth solvent presentation and first MT presentation. Data in black displays mean ± standard error of the mean; grey lines represent individual animals, n=6. *$p < 0.05$.

Validation of complex functions

Valve opening times

Next we sought to validate that our custom-olfactometer can reliably deliver odours across a range of presentation durations.

Using 1ml 5% MT delivered from the same module (Red), to minimise potential inter-module differences, we recorded miniPID responses to ten consecutive presentations at valve opening durations ranging from 10ms to 100ms. Responses at these shorter opening durations did not exhibit the peak-plateau profile observed during the longer (5s, 10s) presentations (Figure 6A and 6B), instead demonstrating more step-like changes (Figure 7A). Across all opening durations, there was minimal trial-to-trial variability in both peak amplitudes (Figure 7Bi; SD: 10ms=1.92, 20ms=2.14, 50ms=1.90, 100ms=2.99, 250ms=4.82, 1000ms=1.63) and latencies (Figure 7Bii; SD: 10ms=2.28, 20ms=0.33, 50ms=1.19, 100ms=1.08, 250ms=2.49, 1000ms=0.57). Peak amplitude increased with valve opening duration (mean: 10ms= 15.85mV, 20ms=24.78mV, 50ms=56.20mV, 100ms=99.24mV, 250ms=101.03mV, 1000ms=81.86mV), reaching maximum values around 100-250ms (Figure 7Ci). Response latencies were similar across most opening durations (mean: 10ms=53.39ms, 20ms=30.99ms, 50ms=38.61ms, 100ms=60.14ms, 250ms=65.27ms, 1000ms=66.33,s), with shorter latencies at 20ms and 50ms (Figure 7Cii).

We then proceeded to confirm that our olfactometer can deliver odours stably during the longer presentation times often required for behavioural experiments (Kobayashi et al., 2008; Ogg et al., 2018; Qiu et al., 2021). Specifically, we wanted to determine whether the small liquid volume used in the odour vials (1 ml) is sufficient to prevent significant signal depletion over longer stimulation durations, and also whether the valves can remain open for extended periods without sporadic closing. To test this, we recorded responses during a continuous 10-min presentation of 1ml 5% MT (Figure 7D). Following the initial peak in signal upon valve actuation, once plateau was reached, the miniPID signal remained stable across the recording with only a very gradual decrease in signal likely indicative of slow odour depletion from the odour bottle.

Together, these results indicate that the olfactometer supports reliable odour delivery across a wide range of protocols, ranging from tens of milliseconds to several minutes, as does, for instance, the commercially-available Aurora 220A olfactometer (Aurora Scientific, 220A), making it suitable for a range of diverse experimental needs.

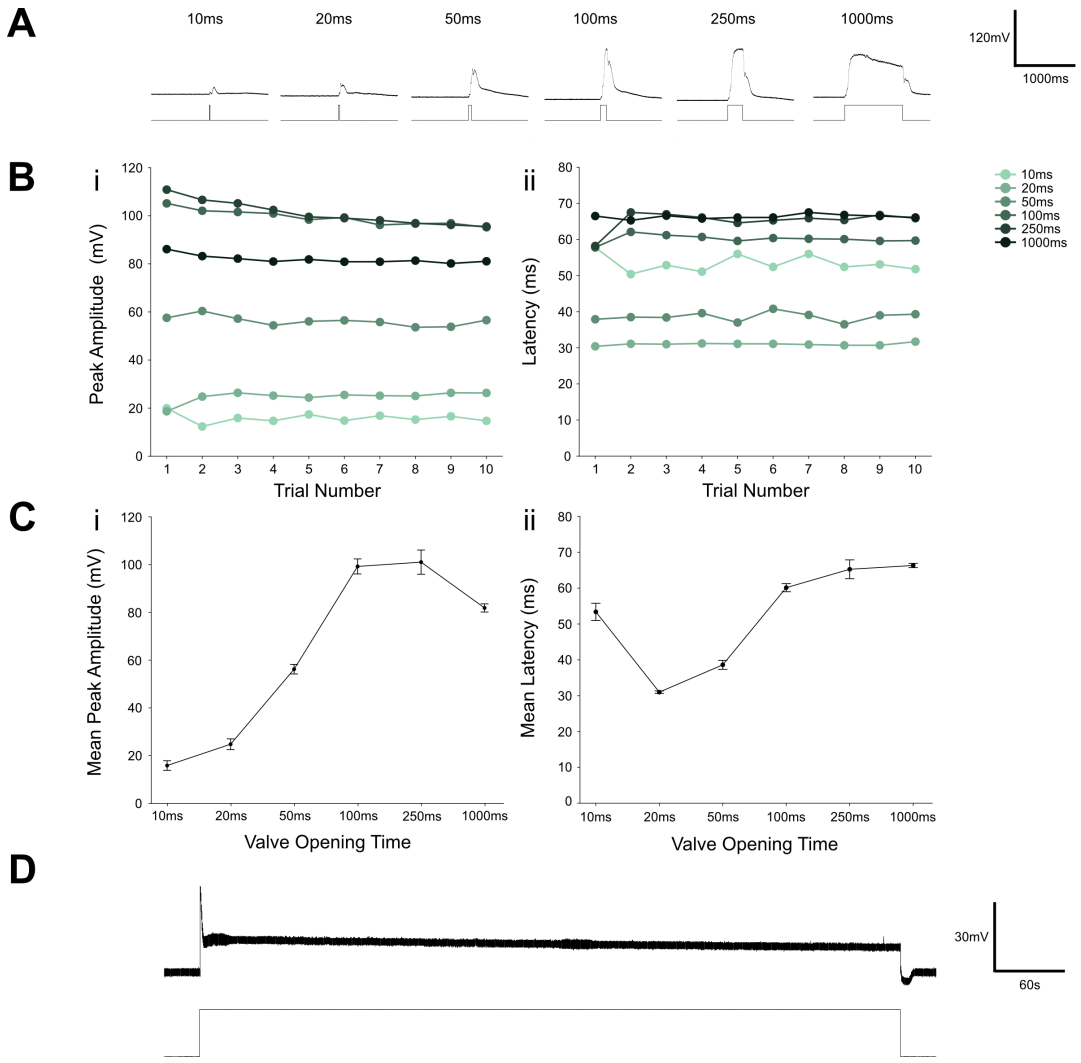

Figure 7. Odour delivery across different valve opening times. (A) Representative traces of 5% MT during presentations of increasing duration. Top: miniPID signal; bottom: digital output voltage trace indicating valve state. (B,C) Quantified features include (i) peak amplitude and (ii) latency from valve actuation to half-peak amplitude. (D) Trace of 5% MT during a 10-min continuous valve opening. Top: miniPID signal; bottom: digital output voltage trace. Error bars represent mean ± SD. All data were acquired from the same odour module.

Concentration range

Assessing the threshold at which subjects are able to detect odorants is a very common and important assay in determining olfactory capabilities, and can provide information about how an experimental manipulations or pathologies have altered the olfactory system (Dewan et al., 2018; Johnson et al., 2023). To test whether our olfactometer can provide sustained and reliable signals at a variety of concentrations we prepared 1ml final volume of MT diluted in solvent at various concentrations ranging from 0.2 to 20% (e.g., 200 µL MT in 800 µL solvent for 20%). We then used the miniPID to record the responses to ten consecutive 10s presentations, with a 15s intertrial interval, at each concentration (Figure 8A). Once more, all solutions were delivered from the same module (Red) to minimise potential inter-module differences in signal.

Across all concentrations, there was minimal trial-to-trial variability in both peak amplitudes (Figure 8Bi; SD: 0.2%=0.28, 0.5%=0.53 ,1%=0.60, 5%=1.25, 10%=3.75, 20%=3.77) and plateau amplitudes (Figure 8Bii; SD: 0.2%=0.15, 0.5%=0.24,1%=0.35, 5%=0.30, 10%=2.33, 20%=3.31), indicating reliable control over the strength of the odorant output. As expected, both peak amplitudes (mean: 0.2%=8.79mV, 0.5%=23.19mV, 1%=25.36mV, 5%=83.86mV, 10%=211.85mV, 20%=367.43mV) and plateau amplitudes (mean: 0.2%=4.58mV, 0.5%=11.57mV, 1%=11.37mV, 5%=25.48mV, 10%=96.49mV, 20%=169.60mV) scaled with odorant concentration (Figure 8Ci-ii), however, the signal remained detectable at the lowest concentration tested. Response latencies were largely stable across concentrations (Figure 8Biii and Ciii; mean ± SD: 0.2%=47.18 ± 8.83ms, 0.5%=60.16 ± 2.61ms, 1%=57.19 ± 2.94ms, 5%=65.72 ± 1.81ms, 10%=57.6 ± 1.39ms, 20%=55.27 ± 1.03ms), with only the lowest concentration (0.2%) showing modest variability.

Together, these results demonstrate that the olfactometer provides reliable and concentration-dependent odour delivery, making it suitable for assays of olfactory sensitivity.

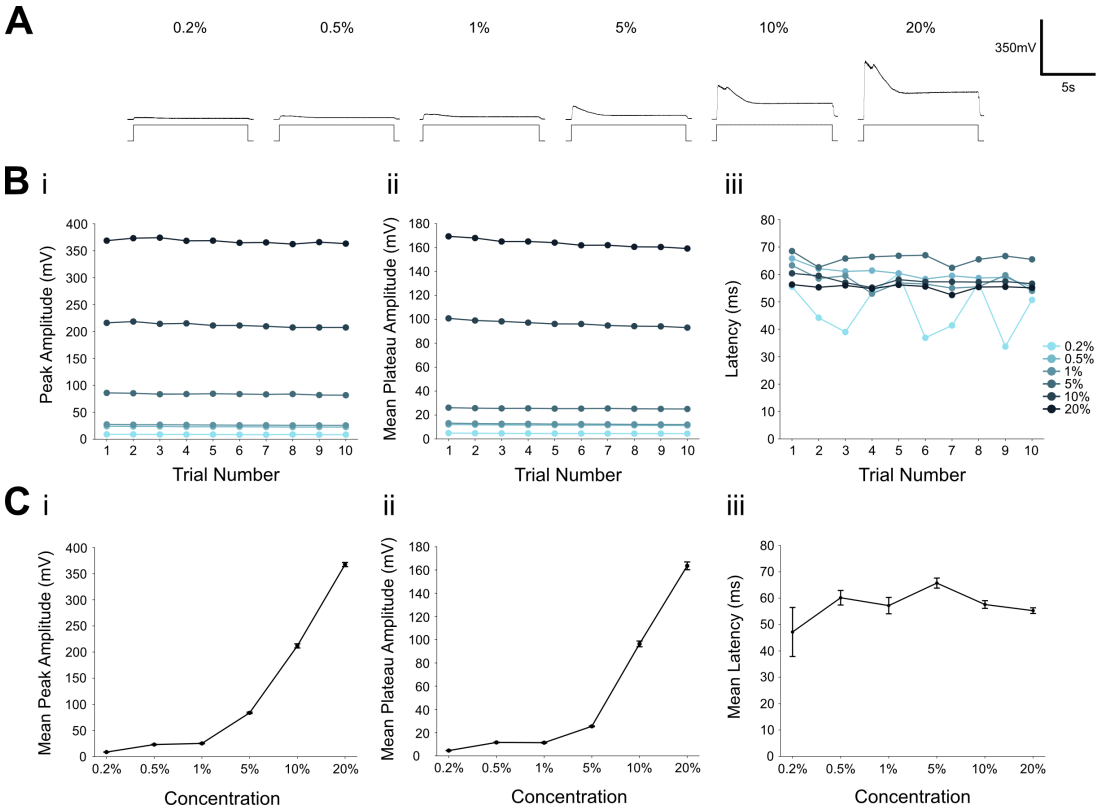

Figure 8. Odour delivery across different concentrations. (A) Representative traces of 0.2, 0.5, 1, 5, 10, and 20% MT from a single module. Top: miniPID signal; bottom: digital output voltage trace indicating valve state. (B,C) Quantified features include (i) peak amplitude, (ii) plateau amplitude, and (iii) latency from valve actuation to peak amplitude. Error bars represent mean ± SD. All data were acquired from the same odour module.

Multiple modules

Our olfactometer consists of four independent modules, allowing the delivery of up to four distinct odours within a single experiment (although this is expandable). The different modules can be activated sequentially, as, for example, in a habituation-dishabituation task where a subject is exposed repeatedly to one odour before being exposed to a new odour (Figure 6C).

While repeated odour delivery from a single module is highly consistent (Figure 6), we next asked whether delivering the same odour across multiple modules would yield similarly consistent results. To test this, we delivered 1 ml of 5% MT from each of the four modules (10s odour presentation, 15s intertrial interval, repeated 10 times per module). The four modules showed similar waveforms, indicating similar odour presentation dynamics across the four modules (Figure 9Ai).

As seen previously, there was minimal trial-to-trial variability in any of the metrics recorded, demonstrating that each of the modules is capable of reliable and consistent odour delivery (Figure 9Aii-iv). Plateau amplitudes were highly consistent across modules (Figure 9Aiii; Red: 7.07 ± 0.28mV, Blue: 11.34 ± 0.19mV, Green: 11.71 ± 0.19mV, White: 12.48 ± 0.36mV), with the Red module displaying a slightly lower plateau. Peak amplitudes were also quite consistent between modules (Figure 9Aii; Red: 35.64 ± 1.87mV, Blue: 28.44 ± 2.88mV, Green: 46.26 ± 2.93mV, White: 44.95 ± 3.68mV), with the Blue module having a slightly lower signal output. Importantly, there wasn't one module with both low peak and plateau amplitudes. Response latencies were very consistent between modules (Figure 9Aiv; Red: 43.36 ± 2.91ms, Blue: 34.66 ± 2.40ms, Green: 47.76 ± 4.72ms, White: 39.7 ± 3.17ms). To evaluate odour depletion and valve stability during prolonged delivery, each module was used to deliver a continuous 60s presentation of 1 ml 5% MT. All four modules produced stable odour signals across the full duration of delivery (Figure 9B), consistent with previous results (Figure 7D)

Together, these findings indicate that odorant delivery is consistent across modules, and each module supports stable odour output over both short and long timescales, enabling their use in sequential odour delivery paradigms.

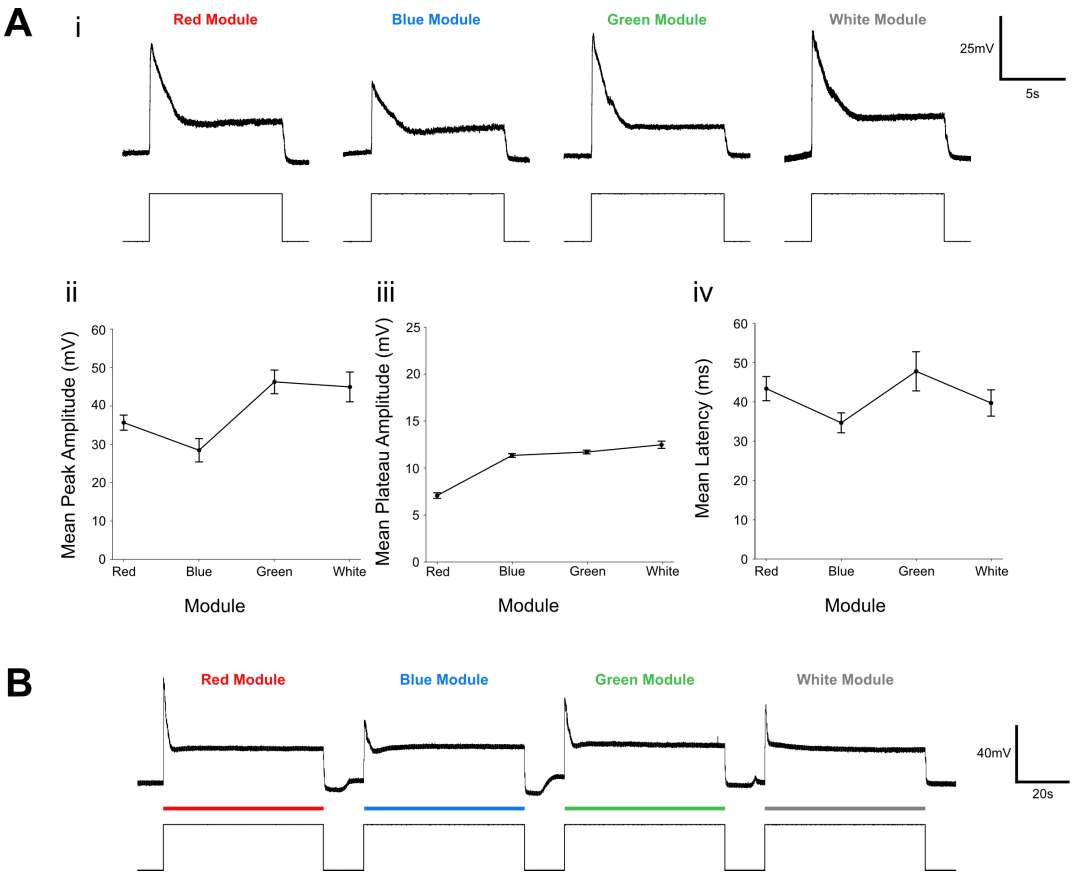

Figure 9. Odour delivery across multiple odour modules. (Ai) Representative traces of 5% MT from all four modules during 10 s presentations with a 15 s inter-stimulus interval. Top: miniPID signal; bottom: digital output voltage trace indicating valve state. (Aii–iv) Quantified features include (i) peak amplitude, (ii) plateau amplitude, and (iii) latency from valve actuation to peak amplitude (ms). (B) Representative traces of 5% MT from all four modules during 60 s presentations. Top: miniPID signal; bottom: digital output voltage trace. Error bars represent mean ± SD.

Odour mixtures

Our system's modular design enables both sequential, as shown above, and simultaneous activation of the four modules, facilitating delivery of odour mixtures for de-mixing and signal-background segregation studies (Rokni et al., 2014; Oleszkiewicz et al., 2018; Reddy et al., 2018; Wilson et al., 2020). Unlike methods that require physical mixing of liquid odorants (Grossman et al., 2008; Hummel et al., 2013), our approach generates mixtures by selectively opening combinations of individual odour bottles, producing vaporised mixtures within the output tubing. This design provides flexibility, permitting real-time manipulation such as initiating delivery with one odour and subsequently adding others.

The traces in Figure 10Ai represent various combinations of 5% MT and 5% ethyl valerate (EV) from two modules, and illustrate that delivering an odour mixture has a greater effect on plateau amplitude than peak amplitude, but also that we have great temporal control over mixture delivery. One issue with generating mixtures in this manner, however, is that there is a difference in the number of bottles open in the single odour (MT or EV) and in the odour mixture (MT + EV) conditions. As a result, since

pressurised air is pumped into and extracted from each bottle in equal amounts, the total pressure delivered at the output stage is greater in the odour mixture condition ("2n") compared to the single odour conditions ("n"; Figure 10Aii). As it is known that olfactory sensory neurons are sensitive to changes in mechanical stimulation (Grosmaitre et al., 2007), this difference in pressure between conditions might confound behavioural and physiological results. To mitigate this, our olfactometer is designed such that at any given time, any module not supplying an odour instead delivers solvent (Figure 10Aiii). This ensures that one bottle from each of the four modules is always open, regardless of the number of odours being presented. For example, when delivering MT only, the remaining three modules deliver solvent; when delivering MT + EV, the remaining two modules deliver solvent. This design should ensure constant pressure regardless of the number of odours being presented.

To verify this, we compared responses across mixtures of increasing complexity, ranging from MT with solvent alone to the full four-odour mixture with no solvent (Figure 10B). Each condition consisted of 10-second odour pulses with 15-second intertrial intervals, repeated over 10 trials. These recordings indicated that pressure remained constant across all conditions (MT + 3 solvent: 5453 ± 860Pa; MT + VAL + 2 solvent: 5534 ± 751Pa; MT + VAL + EV + solvent: 5586 ± 825Pa; MT + VAL + EV + methyl butyrate (MB); 5453 ± 904Pa), confirming that through our design pressure can be effectively stabilized by consistently opening four modules. Expectedly, increasing the proportion of odour channels led to higher peak (MT + 3 solvent: 10.71 ± 0.21mV; MT + VAL + 2 solvent: 20.97 ± 1.35mV; MT + VAL + EV + solvent: 22.74 ± 0.44mV; MT + VAL + EV + MB; 41.85 ± 2.44mV) and plateau (MT + 3 solvent: 8.37 ± 0.13mV; MT + VAL + 2 solvent: 11.31 ± 0.48mV; MT + VAL + EV + solvent: 15.28 ± 0.25mV; MT + VAL + EV + MB; 20.98 ± 1.35mV) amplitudes.

In practice, experimental designs may not always require the simultaneous delivery of four odours. For example, in Figure 10Ai, only two odours are presented as a mixture. In such cases, it is not necessary to open all four bottles; instead, the number of bottles opened should match the maximum number of odours delivered at once in the full experimental series. As shown in Figure 10B, a detectable signal is still obtained when three solvent bottles are co-activated, but to better understand how the number of co-activated solvent bottles alters the odour signal, we tested MT delivery alone and in combination with one, two, or three solvent bottles. Each condition consisted of 10-second odour pulses with 15-second intertrial intervals, repeated over 10 trials. As expected, the addition of solvent channels led to a reduction in peak PID signal (MT alone: 23.8 ± 0.4mV; MT + 1 solvent: 13.2 ± 0.7mV; MT + 2 solvents: 11.5 ± 0.1mV; MT + 3 solvents: 10.7 ± 0.2mV), however, the plateau signal only decreased modestly (MT alone: 11.29 ± 0.30mV; MT + 1 solvent: 9.80 ± 0.47mV; MT + 2 solvents: 9.66 ± 0.10mV; MT + 3 solvents: 8.37 ± 0.13mV). Importantly, peak pressure increased markedly as additional modules were activated (MT alone: 773 ± 137 Pa; MT + 1 solvent: 2135 ± 367 Pa; MT + 2 solvents: 3890 ± 681 Pa; MT + 3 solvents: 5453 ± 860 Pa). This demonstrates that varying the number of active bottles introduces pressure artefacts that may confound experimental results, thereby validating our design strategy of keeping the same number of modules active regardless of the odours being delivered.

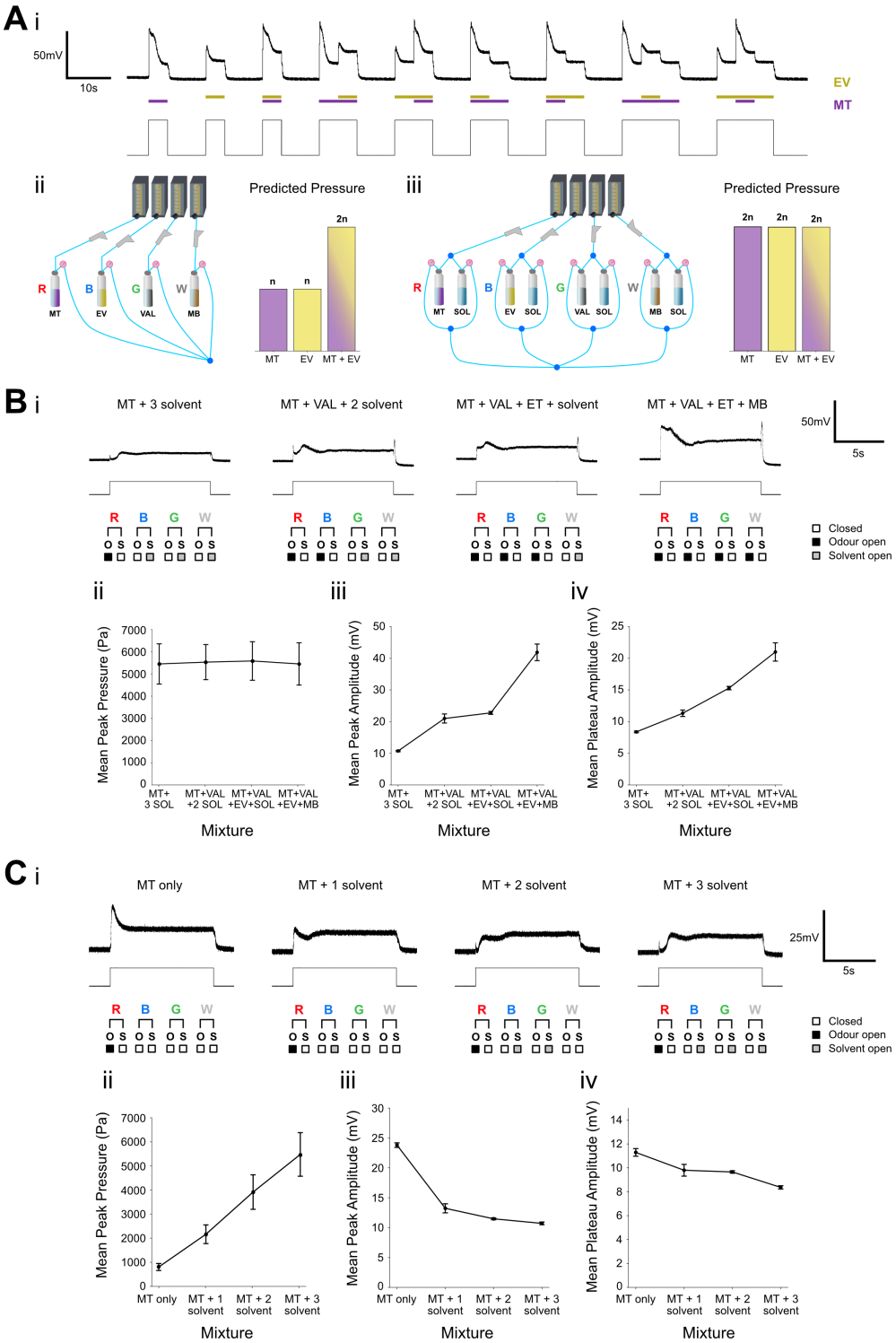

Figure 10. Olfactometer delivery of odour mixtures. Digital voltage pulses and miniPID measurements of combinations of 1 ml 5% ethyl valerate (yellow) and 1 ml 5% MT (purple). (Aii) Olfactometer schematic lacking solvent channels and corresponding predicted pressure during mixture delivery. (Aiii) Our olfactometer schematic and corresponding predicted pressure during mixture delivery. (Bi) Digital voltage pulses, miniPID measurements, and schematic showing which bottles are open during mixture delivery. (Bii–iv) Quantified features include (i) peak pressure, (ii) peak amplitude, and (iii) plateau amplitude. MT, methyl tiglate; VAL, valeraldehyde; EV, ethyl valerate; MB, methyl butyrate; SOL, solvent. (Ci) Digital voltage pulses, miniPID measurements, and schematic showing which bottles are open during mixture delivery. (Cii–iv) Quantified features include (i) peak pressure, (ii) peak amplitude, and (iii) plateau amplitude, averaged across trials for MT with varying numbers of solvent bottles. Error bars represent mean ± SD.

Discussion

We have presented a fully open-source olfactometer adapted for olfactory research on different models and an accompanying behavioural arena for rodent olfactory testing, detailing complete design, materials and assembly guidance. Through extensive validation across multiple experimental paradigms, we confirmed that the system delivers the precision and reliability needed for rigorous olfactory research.

Advantages of using the custom-made olfactometer

Our aim was to develop an olfactometer that is (1) affordable and scalable; (2) simple to assemble without specialised skills or access to mechanical/electronic workshops; (3) easily transportable across testing rooms/setups; (4) operated by fully open-source and customizable software; (5) suitable for a variety of experimental configurations, ranging from human imaging experiments in a scanner, to rodent freely moving and head-fixed behavioural experiments; (6) suitable for multi-subjects setups; (7) capable of delivering both single odours and mixtures while maintaining air pressure constant. Below we detail how we have succeeded in meeting all of these targets.

At the time of writing, the cost of the components for constructing the olfactometer comes to around £1500/ €1700/$2000 (excluding the medical air compressor and desktop PC). Although we describe a four-module configuration, the modular architecture allows straightforward expansion to additional channels, with the only limiting factor being space and the organisation of electronic components and tubing to avoid a tangled and cluttered setup. In terms of construction, the only step requiring specialised tools is soldering wires for the power supply unit. Since soldering is a relatively simple process, with tutorials online and full kits available for less than £30, we consider this olfactometer highly accessible even for researchers with little engineering experience who are new to olfactory studies and/or to setup building. Similarly, the behavioural arenas can be assembled with minimal technical skill, as many of the required parts are commercially available with pre-cut holes. We hope have documented the assembly process in sufficient detail to encourage users to devise alternatives where necessary.

The design itself is compact and modular, with components organised in a way that facilitates transport and reconfiguration across different testing environments. The olfactometer was built on a trolley, with wheel attachments, to ensure maximum mobility, while the behavioural setup described here is placed on a wheeled table. The olfactometer is controlled using the Arduino IDE, this is a fully-open source and customisable software, enabling users to fully specialise their odour delivery protocol to match their specific needs and model.

In line with multiple studies (Johnson and Sobel, 2007; Lundström et al., 2010; Burton et al., 2019) and the technical details of major commercially available olfactometers, we have characterised the parameters that we believe are the most relevant to researchers interested in building their own system. Our validation demonstrates that the olfactometer produces highly consistent outputs across a wide range of conditions, with little to no trial-to-trial variability (*e.g.*, Figure 6Ai). This reliability is essential because absolute values can vary depending on factors such as miniPID placement, tubing length, or chosen flow rate and pressure. Crucially, the olfactometer itself remains consistent, delivering reliable signals from 10ms to 10 minutes (and likely longer). Moreover, outputs are consistent across the four modules, with latencies that are both similar and highly reproducible. These features make the system suitable for use in both human and animal experiments, from imaging in a scanner to rodent head-fixed or freely moving paradigms.

Our behavioural results were obtained using a multi-animal setups to maximise experimental efficiency, eliminating the need to build multiple olfactometers for simultaneous testing of different animals. Because odour is delivered through tubing, the

behavioural boxes can be fully sealed, preventing animals from smelling each other. The use of black IR-plexiglass also prevents visual interaction, ensuring isolation across individuals. This system could readily be adapted for simultaneous human testing. For example, odours could be delivered through 3D-printed masks or commercially available disposable masks with good sealing, such as those used to prevent the spread of respiratory diseases, modified to include a small hole for the odour delivery tube. Finally, a further advantage of this design is its ability to deliver odour mixtures under constant pressure (Rokni et al., 2014; Mathis et al., 2016). Maintaining stable pressure is crucial to prevent odour-combination experiments from being confounded by fluctuations in flow or delivery dynamics. With this system, mixtures can be presented as reliably as single odours, broadening the experimental scope to include more naturalistic and complex olfactory environments. This capability is particularly valuable as recent work shows that different olfactory network mechanisms may emerge depending on task difficulty (Kuruppath et al., 2023).

Limitations and alternatives

Compared with purchasing a commercial olfactometer, our approach requires additional effort in sourcing components, assembling the device, aligning outputs between modules and characterising its performance. We believe this time investment (approximately 3 to 4 weeks) is worthwhile for those seeking greater flexibility to tailor the system to specific experimental needs, reduce overall costs, and avoid dependence on manufacturer support if problems arise. However, laboratories which have the financial resources but are more time-constrained may find commercial systems more suitable.

Another consideration is the profile and amplitude of the odour signal. Compared with some commercial systems, our device produces a lower-amplitude response with a characteristic peak-plateau profile. This means that this device may not be suitable for experiments requiring sharp, step-like or more complex concentration transitions, such as sinusoidal changes in concentration. For example, imaging studies aiming to link stimulus dynamics to rapid neuronal responses could be influenced by the delivery dynamics of our system. However, similar dynamics are found in other olfactometer designs (Reinert et al., 2019; Tichy et al., 2020), and for brief odour presentations (<1 s), the signal from this olfactometer is indeed more square-like.

A further limitation stems from the way odourised air joins a constant carrier stream, increasing the pressure of the output flow. As such, when an odour (or solvent) valve is opened, there is a detectable change in airflow that can be felt as a transient air puff. Although the magnitude of this change is consistent across modules and mixtures (Figure 10Bii), it could still serve as an additional cue in behavioural experiments. For example, subjects might learn to associate the airflow transient rather than the odour itself with reinforcement, potentially confounding the interpretation of olfactory learning or discrimination tasks. However, this is not a significant concern since the airflow transient remains consistent across all modules. Therefore, if a subject shows discrimination behaviour when the bottles are filled with odours and not in probe trials where all bottles are only filled with solvent, one can be confident that it is responding to the odour rather than to airflow changes.

In addition to the air puff, each solenoid valve produces an audible click upon actuation. Although these sounds are reduced by placing the olfactometer relatively far from the testing area (with the caveat of not going too far to avoid an excessively long output tubing, which will cause a drop in pressure) and/or enclosing it in a foam box, auditory cues could still provide unintended signals during behavioural tasks. Such cues may become particularly relevant in learning paradigms, where subjects could associate reinforcement with valve clicks rather than odour identity. The robustness of the behavioural response can be tested again with a probe trial in which the valves are

scrambled, but the subject should still be able to perform correctly (Erskine et al., 2019; Ackels et al., 2021). Furthermore, although the air compressor is usually quite quiet, intermittently it gets quite noisy. It is possible that this extra noise can distract subjects, interfering with their natural behaviour. We have performed miniPID validation while using an oxygen cylinder (data not shown), so, if desired, these can be used as a quieter alternative, but keeping in mind its possibly fast depletion depending of the experimental protocol. We had no access to compressed air from a wall faucet, such as those used to float optical tables, but these could serve as alternative, quieter air sources if they provide clean air at a stable pressure.

As with most olfactometers, contamination remains a potential limitation, as odours can adhere to tubing. To minimise this, tubing must be replaced between experiments, which introduces additional time and modest expense. The inclusion of a continuous carrier path in our design helps to reduce residual odour, but cannot completely eliminate the issue. Researchers should therefore account for tubing replacement and maintenance as part of experimental planning. Finally, for those who do build this olfactometer, we'd encourage them to validate their outputs as thoroughly as possible. The data reported here captures our specific device, and even minor changes in miniPID placement or tubing length could alter the signals obtained. While the validation process may be laborious, and the miniPID is unfortunately not cheap, we consider it a worthwhile investment for ensuring data integrity.

Conclusion

We have aimed to provide a thorough account of our olfactometer design that can serve as a hands-on reference for researchers interested in building something similar. We hope this system, which is affordable, capable of delivering precisely-timed odours, and can be assembled largely from easily obtainable components, proves useful. Our descriptions of the mouse behavioural arenas (which are easily scalable for larger subjects) and recording setup should also serve as helpful guides for those working with olfaction in terrestrial animals and human models. As always with science and technology, we are fully aware that our design certainly has room for improvement and welcome any openly-shared improvement of our design. By reducing the technical and financial barriers to undertake olfactory research, we hope to see more laboratories exploring this fundamental sensory modality that profoundly shapes both human experience and animal behaviour, helping to elevate olfaction from its historical status as the neglected sense to its rightful place at the forefront of sensory neuroscience.

Materials and Methods

Four-module olfactometer parts list

Table 1. Olfactometer parts list

Component category	Part	Supplier (cat. #)	Qty.
Air flow control	Pneumatic pressure regulator	SMC (AR20-F01BG-B)	2
	Flow meter	Key Instruments (25102A13BVBN)	5
	Speed controller	SMC (AS1211F-M5-04)	4
	Solenoid valve	Lee Company (LHDB1262245D)	8
Electronic control	Breadboards	Rapid (R-TECH 34-1330)	6
	Timer circuits	Rapid (Texas Instruments 82-0336)	8
	Capacitor, 680 pF, 50V	Farnell (Vishay 3289410)	8
	Capacitor, 100nF, 50V	CPC (MULTICOMP CA06296)	8
	Capacitor, 0.01µF, 63V	Farnell (KEMET 3784298)	8
	Rectifier diode	RS (Vishay 628-9142)	24
	Zener diode	Farnell (onsemi 2822514)	8
	Darlington Transistor	RS (STMicroelectronics 793-1318)	16
	Transistor	RS (onsemi 739-0505)	16
	Resistor 160k ohm	RS (Vishay 683-3070)	8
	Resistor 10k ohm	Rapid (Royal Ohm 62-7218)	20
	Resistor 330 ohm	RS (Yageo 199-7756)	28
	Resistor 240 ohm	RS (TE Connectivity 148-354)	4
	Resistor 47k ohm	–	4
	Resistor 4.7k ohm	CPC (MULTICOMP MF25 4K7)	8
	Kit of jumper wire	Rapid (K&H Manufacturing 34-0495)	1
	Jumper cable Male to Female connector	Farnell (Pro Signal 2452749)	20
	Jumper wire Male to Male	Farnell (Bud Industries 2762508)	20
	Voltage regulator 5A	RS (Texas 460-900)	4
	Electrolytic Capacitor	RS (707-6278)	4
	Voltage regulator 100mA	RS (Texas Instrument 533-5711)	4
	Plug in Power Supply 12V	CPC (Ideal Power PW04341)	1
	Power Socket to Screw Terminal Adaptor	CPC (Clever Little Box CLB-JL-53)	1
	PCB terminal block	CPC (MULTICOMP MC000034)	1
	Wire	Farnell (Alpha Wire 2290891)	1
Tubing connection	Y Tube to Tube Adaptor push in 6 mm to 6 mm	RS Components (916-0918)	1
	Double Y Tube to Tube Adaptor push in 6 mm to push in 4 mm	Festo (QSQ-6-4)	2
	Y Tube to Tube Adaptor push in 4 mm to 4 mm	RS Components (916-0915)	9
	Straight Threaded Adaptor G1/8 Male to push in to 6 mm	RS Components (299-3819)	3
	Straight Threaded Adaptor G1/8 Male to push in to 4 mm	RS Components (299-3796)	1
	M5 female to push in 4 mm	RS Components (176-1293)	4
	Elbow threaded Adaptor NPT 1/8 Male to push in 5/32 in	SMC (KQ2L03-34AS)	10
	Air Pipe Clear Polyether 6 mm x 25 mm	Legris (1025U06R08)	1
	Air Pipe Clear Polyurethane 4 mm x 30m	RS Components (917-2407)	1
Disposable (1 per odorant tested)	Adapter barbed 3/32 inch I.D. to Luer male	Fisher Scientific Ltd (16894673)	2
	24mm PP Screw Seal, Center hole	Fisher Scientific Ltd (10729454)	1
	EPA Screw Neck Vial, Glass	Fisher Scientific Ltd (11530585)	1
	Syringe needle, 19gx2.0	Appleton Woods Ltd (GS357)	2

We include these product details for reference to aid replication of our design, not as endorsements of specific suppliers. Better or cheaper alternatives may be available elsewhere. Readers should research local suppliers and compare options when sourcing materials.

Behavioural arena parts list

Table 2. Behavioural arena parts list

Component category	Part	Supplier (cat. #)	Qty.
Boxes	Black Cast Perspex Acrylic Sheet (300mm x 300mm x 3mm)	Bay Plastics Ltd (BLACK:962)	2
	Black Cast Perspex Acrylic Sheet (300mm x 205mm x 3mm)	Bay Plastics Ltd (BLACK:962)	1
	Clear Cast Perspex Acrylic Sheet (300mm x 195mm x 3mm)	Bay Plastics Ltd (CLEAR)	1
	Black Cast Perspex Acrylic Sheet (300mm x 200mm x 3mm)	Bay Plastics Ltd (BLACK:962)	2
	Aluminium Angle - 1m length (38mm x 38mm x 3mm)	RS (681-716)	1
	Aluminium profile strut - 1m length - (20mm x 20mm, 5mm groove)	RS (8508476)	1
	Small Kitchen Funnels (3pcs)	Fogcays (3xgf)	2
	Polythene backed absorbent protector sheet (460mm x 570mm)	Benchkote (2300-916)	1
Cameras	1080p Night Vision USB Camera (sideview)	Arducam (B0205)	1
	1080p Night Vision USB Camera (topview)	Svpro (SVB-USBFHD05MT-KL36IR)	1
Camera mounts	Flexible Helping Hands	JZK (M461328U)	1
	Tabletop Camera Mount Stand	NEEWER (TL253A+CR221A)	1
Exhaust Fans	LD10 Linear Diaphragm Pump	Charles Austen Pumps Ltd (X12-810)	1
Tubing and connectors	Air Pipe Clear Polyurethane 4mm x 30m	RS Components (917-2407)	1
	Polyurethane Flexible Tubing 4mm ID, 6mm OD, Clear	RS Components (366-459)	1
	Barbed Connector 3/32 to 3/32 in	Harvard Apparatus (72-1500)	2
	Straight Reducer 1/8 to 3/32 in	Cole-Parmer (5010881)	1

We include these product details for reference to aid replication of our design, not as endorsements of specific suppliers. Better or cheaper alternatives may be available elsewhere. Readers should research local suppliers and compare options when sourcing materials.

Odorants

Odorants were obtained from Sigma-Aldrich (Metyl butyrate, 246093; Valeraldehyde, 110132) or Tokyo Chemical Industry (Methyl tiglate, T0248; Ethyl valerate, V0004). Odorants were diluted in diethyl phthalate solvent (Sigma-Aldrich, 524972) to the desired concentration and a total volume of 1ml. All odour concentrations are reported as volume/volume (v/v). Dilutions were prepared immediately before each miniPID recording or behavioural experiment.

Odour delivery

In all miniPID and behavioural experiments air was supplied via a medical air compressor (MGF compressors, S-OF100-003-MS2). Air was passed through two pressure regulators (one for carrier path, one for odour and solvent path) set to 0.2MPa. Carrier path flowmeter was set to 1L/min and the four odour path flowmeters were set to 0.3/min. Odour delivery was controlled using an Arduino-compatible microcontroller board (AZ-Delivery, AZ-ATmega328) programmed with a custom Arduino IDE script. Digital output pins from the microcontroller were interfaced with valve driver boards to precisely control valve activation timing and duration.

Odour delivery validation and pressure recordings

Odour delivery was confirmed and quantified using a mini photoionization detector (miniPID 200B; Aurora Scientific) positioned at the odour port of one behavioural arena. The miniPID was allowed to warm up for at least 30min before recording. Valve openings were simultaneously recorded by monitoring the digital output voltage (0V/5V) from the Arduino via a Digidata 1332A (Axon Instruments) and captured with Clampex 9.2 (Molecular Devices). Unless multiple modules were involved, all recordings used odours from the same module (Red) to minimize variability in pressure, flow, or odorant preparation. MiniPID traces were analyzed in Clampfit (v11.3). From each trace, using built-in Clampfit analysis cursors, we extracted peak amplitude (maximum during valve opening), plateau amplitude (mean from 5s post-opening to valve closure), and latency (time in ms from valve opening to half-maximal response). Pressure was monitored with a digital manometer (Danoplus DP-103), with readings extracted from video recordings of valve operation captured by a USB camera. Peak pressure was determined as the highest manometer reading during valve opening.

To quantify odour delivery with a commercially available olfactometer (CyNexo srl., Sniff-0), odours were prepared by pipetting 500 µL onto a cotton pad, following the manufacturer's instructions. Sniff-0 miniPID recordings were also analysed in Clampfit (v11.3). Because valve actuation timings were not recorded by the Sniff-0 software, latency could not be quantified. Additionally, traces from the Sniff-0 system showed a square-shaped response rather than the peak–plateau profile observed with our custom olfactometer, and recordings were limited to 2s valve openings. Therefore, only peak amplitude was extracted for these recordings.

Mouse behavioural testing and analysis

Mice of either sex, aged 2 to 5 months, were housed under a 12 h light/dark cycle in an environmentally controlled room with ad libitum access to food and water. In line with the 3R principles, we used both wild-type mice (C57Bl/6J; Charles River Laboratories) and surplus animals from transgenic breedings [DATIREScre (B6.SJL-Slc6a3tm1.1(cre)Bkmn/J, Jax stock #006660], Ai9 [B6.Cg Gt(ROSA)26Sortm9(CAG-tdTomato)Hze/J; Jax stock #007909)], and TRAP [Fostm2.1(icre/ERT2)Luo/J; Jax

stock #030323]) ongoing in the laboratory. The integrity of the transgenic lines was ensured by generating breeders via back-crossing heterozygous carriers with C57Bl6 animals specifically bought biannually from Charles Rivers Laboratories. All experiments were performed at the University of Cambridge in accordance with the Animals (Scientific procedures) Act 1986 and with AWERB (Animal Welfare and Ethical Review Board) approval.

Following protocols adapted from Qiu et al., (2014) and Conway et al., (2024), mice were placed inside behavioural arenas and habituated to carrier airflow before testing. Odour delivery consisted of five 1-min presentations of solvent, each separated by 30s intertrial intervals, followed by three 1-min presentations of 5% MT (Figure 6C). The total session lasted 12 minutes. Valve timing was controlled by an Arduino-compatible microcontroller, and odour periods were signalled by an LED light visible to the camera. Mice were tested in a 30×20×30cm arena made of black IR-transmitting plexiglass, allowing infrared video recording while limiting visual distractions. A mini-funnel was installed 5cm from the base of one short wall to deliver odour via the olfactometer. An exhaust tube on the opposite wall removed residual odour via an extractor pump (Charles Austen Pumps Ltd, LD10).

Behaviour was recorded at 20fps using an IR USB camera top-down using Bonsai-Rx (Lopes et al., 2015). All testing was conducted in darkness or red light. Body tracking was performed in DeepLabCut (Mathis et al., 2018), using the superanimals_topviewmouse model from Modelzoo (Ye et al., 2024). The data from seven body parts were extracted and fed into SimBA (Goodwin et al., 2024) for behavioural quantification. A circular region of interest (ROI) with radius 3cm was drawn centred on the odour port. Investigation time was calculated by taking the time spent with the nose located within the ROI. Statistical analyses were performed using RStudio (version 4.5.0). Data normality was assessed using the Shapiro-Wilk test, with parametric or nonparametric tests applied accordingly. Statistical significance was set at $\alpha = 0.05$ for all two-tailed comparisons.

Author Contributions

CD: Conceptualization, Investigation, Validation, Formal analysis, Data curation, Visualization, Writing – original draft, Writing – review & editing

JW: Conceptualization, Investigation, Writing – review & editing

EG: Conceptualization, Investigation, Visualization, Funding acquisition, Project administration, Supervision, Writing – original draft, Writing – review & editing

CG: Conceptualization, Investigation, Validation, Formal analysis, Data curation, Funding acquisition, Project administration, Writing – original draft, Writing – review & editing

The authors declare no financial or personal relationship which could be construed as a potential conflict of interest.

Acknowledgements

This work was supported by project grants from the URKI Biotechnology and Biological Sciences Research Council (BB\W014688\1), the Newton Trust, and the Wellcome Trust (301427/Z/23/Z) (EG); a CyNexo Young Investigator Award (CG); and a Harding Distinguished Postgraduate scholarship (CD). We wish to thank Dan Rokni, Tobias Ackels, Tom Oldham and Glenn Harrison for their invaluable insights during the olfactometer designing and validating stages, Jasper Poort for software advice, Ailie McWhinnie and Harin Wijayathunga for comments on the manuscript, and all members of the Galliano laboratory for providing helpful discussions.

References

Ackels T, Erskine A, Dasgupta D, Marin AC, Warner TPA, Tootoonian S, Fukunaga I, Harris JJ, Schaefer AT (2021) Fast odour dynamics are encoded in the olfactory system and guide behaviour. Nature 593:558–563.

Arevalo N, Mettetal MR, Quinones FJ, Restrepo D, Ramirez-Gordillo D (2025) Constructing an Olfactometer for Rodent Olfactory Behavior Studies. Journal of Visualized Experiments (JoVE) : e67049.

Bodyak N, Slotnick B (1999) Performance of mice in an automated olfactometer: odor detection, discrimination and odor memory. Chem Senses 24:637–645.

Burton SD, Wipfel M, Guo M, Eiting TP, Wachowiak M (2019) A Novel Olfactometer for Efficient and Flexible Odorant Delivery. Chemical Senses 44:173–188.

Conway M, Oncul M, Allen K, Zhang Z, Johnston J (2024) Perceptual constancy for an odor is acquired through changes in primary sensory neurons. Science Advances 10:eado9205.

Dewan A, Cichy A, Zhang J, Miguel K, Feinstein P, Rinberg D, Bozza T (2018) Single olfactory receptors set odor detection thresholds. Nat Commun 9:2887.

Erskine A, Ackels T, Dasgupta D, Fukunaga I, Schaefer AT (2019) Mammalian olfaction is a high temporal bandwidth sense. bioRxiv doi: 10.1101/570689

Goodwin NL, Choong JJ, Hwang S, Pitts K, Bloom L, Islam A, Zhang YY, Szelenyi ER, Tong X, Newman EL, Miczek K, Wright HR, McLaughlin RJ, Norville ZC, Eshel N, Heshmati M, Nilsson SRO, Golden SA (2024) Simple Behavioral Analysis (SimBA) as a platform for explainable machine learning in behavioral neuroscience. Nat Neurosci 27:1411–1424.

Grosmaitre X, Santarelli LC, Tan J, Luo M, Ma M (2007) Dual functions of mammalian olfactory sensory neurons as odor detectors and mechanical sensors. Nat Neurosci 10:348–354.

Grossman KJ, Mallik AK, Ross J, Kay LM, Issa NP (2008) Glomerular activation patterns and the perception of odor mixtures. Eur J Neurosci 27:2676–2685.

Hummel T, Olgun S, Gerber J, Huchel U, Frasnelli J (2013) Brain responses to odor mixtures with sub-threshold components. Front Psychol 4:786.

Ishii KK, Touhara K (2019) Neural circuits regulating sexual behaviors via the olfactory system in mice. Neuroscience Research 140:59–76.

Johnson BN, Sobel N (2007) Methods for building an olfactometer with known concentration outcomes. J Neurosci Methods 160:231–245.

Johnson CE, Williams E, Dewan A (2023) Protocol for quantifying the odor detection threshold of mice. STAR Protocols 4:102635.

Kobayashi T, Sakai N, Kobayakawa T, Akiyama S, Toda H, Saito S (2008) Effects of cognitive factors on perceived odor intensity in adaptation/habituation processes: from 2 different odor presentation methods. Chem Senses 33:163–171.

Kohl J, Autry AE, Dulac C (2017) The neurobiology of parenting: A neural circuit perspective. Bioessays 39:1–11.

Kuruppath P, Xue L, Pouille F, Jones ST, Schoppa NE (2023) Hyperexcitability in the olfactory bulb and impaired fine odor discrimination in the Fmr1 KO mouse model of fragile X syndrome. J Neurosci:JN-RM-0584-23.

Lopes G, Bonacchi N, Frazão J, Neto JP, Atallah BV, Soares S, Moreira L, Matias S, Itskov PM, Correia PA, Medina RE, Calcaterra L, Dreosti E, Paton JJ, Kampff AR (2015) Bonsai: an event-based framework for processing and controlling data streams. Front Neuroinform 9:7.

Lopes G, Monteiro P (2021) New Open-Source Tools: Using Bonsai for Behavioral Tracking and Closed-Loop Experiments. Front Behav Neurosci 15:647640

Lorig TS, elmes DG, Zald DH, Pardo JV (1999) A computer-controlled olfactometer for fMRI and electrophysiological studies of olfaction. Behavior Research Methods, Instruments, & Computers 31:370–375.

Lundström JN, Gordon AR, Alden EC, Boesveldt S, Albrecht J (2010) Methods for building an inexpensive computer-controlled olfactometer for temporally precise experiments. Int J Psychophysiol 78:179–189.

Majid A, Burenhult N (2014) Odors are expressible in language, as long as you speak the right language. Cognition 130:266–270.

Mathis A, Mamidanna P, Cury KM, Abe T, Murthy VN, Mathis MW, Bethge M (2018) DeepLabCut: markerless pose estimation of user-defined body parts with deep learning. Nat Neurosci 21:1281–1289.

Mathis A, Rokni D, Kapoor V, Bethge M, Murthy VN (2016) Reading Out Olfactory Receptors: Feedforward Circuits Detect Odors in Mixtures without Demixing. Neuron 91:1110–1123.

McGann JP (2017) Poor human olfaction is a 19th-century myth. Science 356:eaam7263.

Nguyen QAT, Rocha A, Chhor R, Yamashita Y, Stadler C, Pontrello C, Yang H, Haga-Yamanaka S (2024) Hypothalamic representation of the imminence of predator threat detected by the vomeronasal organ in mice Wassum KM, ed. eLife 12:RP92982.

Ogg MC, Ross JM, Bendahmane M, Fletcher ML (2018) Olfactory bulb acetylcholine release dishabituates odor responses and reinstates odor investigation. Nat Commun 9:1868.

Oleszkiewicz A, Rambacher L, Whitcroft KL, Hummel T (2018) The confounding effect of background odors on olfactory sensitivity testing. Journal of Neuroscience Methods 306:88–91.

Park S, Whang M (2018) Infrared Camera-Based Non-contact Measurement of Brain Activity From Pupillary Rhythms. Front Physiol 9:1400

Qiu Q, Scott A, Scheerer H, Sapkota N, Lee DK, Ma L, Yu CR (2014) Automated Analyses of Innate Olfactory Behaviors in Rodents. PLOS ONE 9:e93468.

Qiu Q, Wu Y, Ma L, Xu W, Hills M Jr, Ramalingam V, Yu CR (2021) Acquisition of innate odor preference depends on spontaneous and experiential activities during critical period Liberles S, Sengupta P, Meeks JP, eds. eLife 10:e60546.

Reddy G, Zak JD, Vergassola M, Murthy VN (2018) Antagonism in olfactory receptor neurons and its implications for the perception of odor mixtures Rieke F, ed. eLife 7:e34958.

Reinert JK, Schaefer AT, Kuner T (2019) High-Throughput Automated Olfactory Phenotyping of Group-Housed Mice. Front Behav Neurosci 13:267

Rokni D, Hemmelder V, Kapoor V, Murthy VN (2014) An olfactory cocktail party: figure-ground segregation of odorants in rodents. Nat Neurosci 17:1225–1232.

Sezille C, Messaoudi B, Bertrand A, Joussain P, Thévenet M, Bensafi M (2013) A portable experimental apparatus for human olfactory fMRI experiments. Journal of Neuroscience Methods 218:29–38.

Shepherd GM (2005) Perception without a thalamus how does olfaction do it? Neuron 46:166–168. Tichy H, Zeiner R, Traunmüller P, Martzok A, Hellwig M (2020) Developing and testing of an air dilution flow olfactometer with known rates of concentration change. J Neurosci Methods 341:108794.

Turner W (1890) The Convolutions of the Brain: A Study in Comparative Anatomy. J Anat Physiol 25:105–153.

Wilson DA, Fleming G, Vervoordt SM, Coureaud G (2020) Cortical processing of configurally perceived odor mixtures. Brain Res 1729:146617.

Xydakis MS, Albers MW, Holbrook EH, Lyon DM, Shih RY, Frasnelli JA, Pagenstecher A, Kupke A, Enquist LW, Perlman S (2021) Post-viral effects of COVID-19 in the olfactory system and their implications. The Lancet Neurology 20:753–761.

Ye S, Filippova A, Lauer J, Schneider S, Vidal M, Qiu T, Mathis A, Mathis MW (2024) SuperAnimal pretrained pose estimation models for behavioral analysis. Nat Commun 15:5165.

Zou J, Wang W, Pan Y-W, Lu S, Xia Z (2015) Methods to measure olfactory behavior in mice. Curr Protoc Toxicol 63:11.18.1-11.18.21.